Study of Hybrid Intelligent Controller for Interior Permanent Magnet Synchronous Motor Drive.

By

AbhijitShaha

A project/thesis in partial fulfillment of the requirements for the degree of
Master of Science
in Electrical and Electronic Engineering

Khulna University of Engineering & Technology
Khulna 920300, Bangladesh
September 2013

Declaration

This is to certify that the thesis work entitled *"**Study of Hybrid Intelligent Controller for Interior Permanent Magnet Synchronous Motor Drive"***has been carried out by *AbhijitShaha* in the Department of *Electrical and Electronic Engineering*, Khulna University of Engineering & Technology, Khulna, Bangladesh. The above thesis work or any part of this work has not been submitted anywhere for the award of any degree or diploma.

Signature of Supervisor

Signature of Candidate

Approval

This is to certify that the thesis work submitted by *AbhijitShaha* entitled *"**Study of Hybrid Intelligent Controller for Interior Permanent Magnet Synchronous Motor Drive"***has been approved by the board of examiners for the partial fulfillment of the requirements for the degree of *Master of Science*in the Department of *Electrical & Electronic Engineering*, Khulna University of Engineering & Technology, Khulna, Bangladesh in December 2013.

BOARD OF EXAMINERS

1. _____
   Prof. Dr. Md. AbdurRafiq — Chairman
   Department ofElectrical & Electronic Engineering (Supervisor)
   Khulna University of Engineering & Technology

2. _____
   Head
   Department of Electrical & Electronic Engineering — Member
   Khulna University of Engineering & Technology

3. _____
   Prof. Dr. Bashudeb Chandra Ghosh
   Department of Electrical & Electronic Engineering — Member
   Khulna University of Engineering & Technology

4. _____
   Prof. Dr. Md. Sahjahan
   Department of Electrical & Electronic Engineering — Member
   Khulna University of Engineering & Technology

5. _____
   Prof. Dr. MirzaGolamRabbani
   Department of Electrical & Electronic Engineering — Member
   EasternUniversity, Bangladesh (External)

Acknowledgements

I wish to express my most sincere gratitude to my supervisor, Professor Dr. Md. AbdurRafiq, for the substantial guidance and support given in scientific writing, and for the valuable opinions expressed during the year. His creative thinking, knowledge and expertise on electric machines and controls are the “Feedback” of my conducted researches.

Special thanks go to Professor Dr. Bashudeb Chandra Ghosh for providing preliminary directions including initial literature on the subject, and for pointing out valuable comments.

Special thanks go to Assistant Professor Kalyan Kumar Halder for providing preliminary algorithm code and papers.

I acknowledge with my gratitude the help ofAssistant Prof. Md. Habibullahwho have always been willing to discuss and exchange ideas.

I would like to thank to the Head of the Department of Electrical and Electronic Engineering for providing me all possible facilities without which I could not think of the completion of research work.

Last but not the least, I am always indebted to all my family members for their endless support and love. I greatly appreciate the sacrifices they have made over the years,without which the completion of my study would not be possible.

Khulna, 25.09.2013

AbhijitShaha

Abstract

In this study, Genetic Algorithm (GA) based high performance control of synchronous motor is proposed whose rotor flux is estimated by evolutionary algorithm learning based Artificial Neural Network (ANN). Fast dynamic speed response is obtained through maintaining the rotor flux constant as in the case of field orientation realistic representation in the analysis. Genetic Algorithm (GA) based proportional- integral (PI) controller tuning is used for getting optimized gain coefficients of PI controller which also help us to get fast speed response synchronous motor drive. The performance of the drive system with GA based PI controller is compared with general algorithm based PI controller. A high performance simple speed estimator is presented in here. There is no speed fluctuation in the speed response of GA based synchronous motor drive under steady state condition when K_p is fixed whereas a little bit speed fluctuation is presented in the GA based synchronous motor drive under steady state condition when K_p is variable. In general, there is no speed fluctuation in the speed response of general algorithm based PI controller. But Genetic Algorithm is more fast performance than general algorithm.

A simulation model of the drive system is developed and used in this study. The motor equations are written in rotor fixed d-q reference frame. A Proportional plus Integral (PI) controller is used to process the speed error to generate the reference torque current. The RNN estimator is used to estimate stator flux components along the stator fixed stationary axes (α-β) Hysteresis current controller block controls the switching of the three phase inverter to apply voltage to the motor stator. Numerical simulation is carried out in order to verify the effectiveness of the proposed control system. Simulation studies show that the proposed RNN estimator can be used to accurately measure the motor fluxes and rotor angle over a wide speed range. The robustness of the drive system is tested for different operating conditions, i.e., sudden load torque change, parameter deviation, speed reversal, ramp change of speed, load disturbance, presence of computational error, etc. The control system is found to work acceptably under these conditions. It is also simple and low cost to implement in a practical environment.

Dedicated

To

My Beloved Parents

&

Respected Teachers

Contents

LIST OF TABLES

LIST OF FIGURE

NOMENCLATURE

$\overrightarrow{v_s}$, $\overrightarrow{i_s}$, $\overrightarrow{\lambda_s}$	Complex space vectors of the three phase stator voltages, currents, and flux linkages
v_s , v_s , v_s	Three phase stator instantaneous phase voltages
i_s , i_s , i_s	Three phase stator instantaneous phase currents
λ_s , λ_s , λ_s	Three phase stator flux linkages
r_a, r_b, r_c	Three phase stator resistances
L_a , L_b , L_c	Self-inductances of the stator a-b-c phase
L_a , L_b , L_a	Mutual inductances between the a-b-c phase
λ_r , λ_r , λ_r	Flux linkages in stator a-b-c windings changing with rotor angle
r_s	Resistance of the stator winding
λ_r	Peak flux linkage due to the permanent magnent
k_e	Back- EMF constant
L_{ls}	Leakage inductance of stator winding due to armature leakage flux
L_m	Inductance fluctuation due to the rotor position dependent on flux
L_c	Average inductance due to the space fundamental air-gap flux
L_s	Stator inductance matrix
θ_r	Rotor angle
λ_d, λ_q	d-and q- axis stator flux linkages
L_d, L_q	d-and q- axis stator synchronous inductances
L_m , L_m	Common mutual inductances on the d- axis and q- axis circuits
P	Derivative of time
ω_r	Angular velocity
α,β	Orthogonal axes of stationary reference frame

d-q	Synchronously rotating reference frame
a,a^2	Spatial operation of the stator windings
P_p	Number of pole pairs
P_i	Instantaneous input power
v_d, v_q	d- and q- axis stator voltage components
i_d, i_q	d- and q- axis stator current components
ω_m	Angular speed of the motor
T_L	Load torque
B_m	Rotational damping co efficient
J_m	Moment of inertia
$[v_s]$	Three phase applied voltages in matrix form
$[i_s]$	Three phase stator currents in matrix form
$[\lambda_s]$	Three phase stator flux linkages in matrix form
$i_{\alpha s}, i_{\beta s}$	α- and β- axis stator current components
$\lambda_{\alpha s}, \lambda_{\beta s}$	α- and β- axis stator flux linkages
E_w	Speed error
i_a^*, i_b^*, i_c^*	Three phase stator reference currents
i_m^*, i_t^*	Magnetizing and torque producing stator current components
ω_r	Motor command speed
K_p, K_i	PI gain
b_k	Bias of the neuron k
x_m	Input signal of the neuron k to m
ω_k	Synaptic weight of the neuron k to m
u_k	Linear combiner output due to the input signals

$\phi(.)$	Activation function
y_k	Output signal of the neuron k
X(n)	Signal vector at the time step n
$\xi(n)$	Cost function at the time step n
$\Lambda_j(n)$	Partial derivative matrix of the state vector x (n) with respect to the weight vector w_j
$U_j(n)$	q- by- (q+m+1) matrix whose rows are all zero
$\phi(n)$	q-by- q diagonal matrix whose *k*th diagonal element is partial derivative of the activation function with respect to its argument
$\xi(n)$	The (q+m+1) –by-1 vector
ΔW_j	Adjustment for the weight vector of the*j*th neuron
$\tilde{y}(n)$	Desired output vector
Z^{-1}	Unit-delay operator
G	Gain function
T_s	Sampling time
η	Rate of learning
τ	Time constant

CHAPTER I

Introduction

1.1 Introduction

Interior Permanent Magnet (IPM) Synchronous Motors are widely used in low and mid power applications such as computer peripheral equipments, robotics, adjustable speed drives and electric vehicles.

The growth in the market of IPM motor drives has demanded the need of simulation tools capable of handling motor drive simulations. Simulations have helped the process of developing new systems including motor drives, by reducing cost and time. Simulation tools have the capabilities of performing dynamic simulations of motor drives in a visual environment so as to facilitate the development of new systems.

A closed loop control system with a PI controller in the speed loop has been designed to operate in constant torque and flux weakening regions. A comparative study of hysteresis control schemes associated with current controllers has been made in terms of harmonic spectrum.

1.2 Motivation

Modeling and simulation is usually used in designing IPM drives compared to building system prototypes because of the cost. Having selected all components, the simulation process can start to calculate steady state and dynamic performance and losses that would have been obtained if the drive were actually constructed. This practice reduces time, cost of building prototypes and ensures that requirements are achieved.

In works available until now ideal components have been assumed in the inverter feeding the motor. The voltages and currents in different parts of the inverter have not been obtained and hence the losses and efficiency cannot be calculated. In this work, the simulation of an IPM motor drive system is developed using Genetic Algorithm. This enables the calculation of currents and voltages in different parts of the inverter and motor under transient and steady conditions.

A hybrid genetic-based proportional–integral (PI) controller for an interior permanent-magnet synchronous motor drive is presented in [1]. At each operating condition a genetic algorithm is used to optimize the PI controller parameters in a closed-loop vector control scheme. The PI controller parameters have been optimized offline using a GA with a performance index to reflect the minimum settling time, minimum overshoot/undershoot, and zero steady-state error [2].

Real Time Recurrent Neural Network (RTRNN) has been used in AC drive systems because of their adaptive, learning and observing function talentless. In [3] proposed a speed and position

estimation algorithm for IPMSM drives was presented. This algorithm utilized the stator voltages and currents measured from the IPMSM drive to obtain the estimated speed.

A speed controller has also been designed for closed loop operation of the drive. Design method for the PI controller is also given. Most of the previous researches on IPMSM drives were carried out either to remove the position and to reduce the three phase inverter size for cost effective and reliable operation.

The main objective of this project work is to investigate the performance of a 4S3P inverter fed IPMSM drive without a position sensor. The specific objectives of the research work are as follows:

- Propose a 4S3P inverter for the IPMSM drive
- Develop a complete vector control scheme for the IPMSM using hysteresis current controller.
- Develop a RNN based adaptive integration methodology for stator flux position estimation for fast response.
- Optimize the PI controller parameters using GA.

1.3 Previous Work

IPM motor drives have been a topic of interest for the last twenty years. Different authors have carried out modeling and simulation of such drives.

In 1986 Sebastian, T., Slemon, G. R. and Rahman, M. A. [4] reviewed interior permanent magnet synchronous motor advancements and presented equivalent electric circuit models for such motors and compared computed parameters with measured parameters.

In 1986 Jahns, T.M., Kliman, G.B. and Neumann, T.W. [5] discussed that interior permanent magnet (IPM) synchronous motors possessed special features for adjustable speed operation which distinguished them from other classes of ac machines. They were robust high power density machines capable of operating at high motor and inverter efficiencies over wide speed ranges, including considerable range of constant power operation. The magnet cost was minimized by the low magnet weight requirements of the IPM design. The impact of the buried magnet configuration on the motor's electromagnetic characteristics was discussed. The rotor magnetic saliency preferentially increased the quadrature-axis inductance and introduced a reluctance torque term into the IPM motor's torque equation. The electrical excitation requirements for the IPM synchronous motor were also discussed. The control of the sinusoidal phase currents in magnitude and phase angle with respect to the rotor orientation provided a means for achieving smooth responsive torque control. A basic feed forward algorithm for executing this type of current vector torque control was discussed, including the implications of current regulator saturation at high speeds. The key results were illustrated using a combination of simulation and prototype IPM drive measurements.

In 1988 Pillay and Krishnan, R. [6], presented IPM motor drives and classified them into two types such as permanent magnet synchronous motor drives (IPMSM) and brushless dc motor

(BDCM) drives. The IPMSM has a sinusoidal back emf and requires sinusoidal stator currents to produce constant torque while the BDCM has a trapezoidal back emf and requires rectangular stator currents to produce constant torque. The IPMSM is very similar to the wound rotor synchronous machine except that the PMSM that is used for servo applications tends not to have any damper windings and excitation is provided by a permanent magnet instead of a field winding. Hence the d, q model of the IPMSM can be derived from the well known model of the synchronous machine with the equations of the damper windings and field current dynamics removed. Equations of the IPMSM are derived in rotor reference frame and the equivalent circuit is presented without dampers. The damper windings are not considered because the motor is designed to operate in a drive system with field-oriented control.

As an extension of his previous work, Pillay, P. and Krishnan, R. in 1989 [7] presented the interior permanent magnet synchronous motor (IPMSM) which was one of several types of permanent magnet ac motor drives available in the drives industry. The motor had a sinusoidal flux distribution. The application of vector control as well as complete modeling, simulation, and analysis of the drive system were given. State space models of the motor and speed controller and real time models of the inverter switches and vector controller were included. The machine model was derived for the IPMSM from the wound rotor synchronous motor.

Morimoto, S., Tong, Y., Takeda, Y. and Hirasa, T. in 1994 [8], the aimed to improve efficiency in permanent magnet (PM) synchronous motor drives. The controllable electrical loss which consisted of the copper loss and the iron loss could be minimized by the optimal control of the armature current vector. The control algorithm of current vector minimizing the electrical loss was proposed and the optimal current vector could be decided according to the operating speed and the load conditions. The operating characteristics controlled by the loss minimization control genetic algorithm were examined in detail by computer simulations results.

In 1997 by Wijenayake, A.H. and Schmidt, P.B. [9], described the development of a two-axis circuit model for interior permanent magnet synchronous motor (IPMSM) by taking machine magnetic parameter variations and core loss into account. The circuit model was applied to both surface mounted magnet and interior permanent magnet rotor configurations. A method for on-line parameter identification scheme based on no-load parameters and saturation level, to improve the model, was discussed in detail. Test schemes to measure the equivalent circuit parameters, and to calculate saturation constants which govern the parameter variations were also presented.

In 1997 Jang-Mok, K. and Seung-Ki, S. [10], proposed a novel flux-weakening scheme for an Interior Permanent Magnet Synchronous Motor (IPMSM). It was implemented based on the output of the synchronous PI current regulator reference voltage to PWM inverter. The on-set of flux weakening and the level of the flux were adjusted inherently by the outer voltage regulation loop to prevent the saturation of the current regulator. Attractive features of this flux weakening scheme included no dependency on the machine parameters, the guarantee of current regulation at any operating condition, and smooth and fast transition into and out of the flux weakening mode. Experimental results at various operating conditions including the case of detuned parameters were presented to verify the feasibility of the proposed control scheme.

Bose, B. K., in 2001 [11], presented different types of synchronous motors and compared them to induction motors. The modeling of IPM motor was derived from the model of salient pole synchronous motor. All the equations were derived in synchronously rotating reference frame and were presented in the matrix form. The equivalent circuit was presented with damper windings and the permanent magnet was represented as a constant current source. Some discussions on vector control using voltage fed inverter were given.

Bowen, C., Jihua, Z. and Zhang, R. in 2001 [12], addressed the modeling and simulation of interior permanent magnet synchronous motor supplied from a six step continuous inverter based on state space method. The motor model was derived in the stationary reference frame and then in the rotor reference frame using Park transformation. The simulation results obtained showed that the method used for deciding initial conditions was very effective.

In 2002 Mademlis, C. and Margaris, N. [13], presented an efficiency optimization method for vector-controlled interior permanent-magnet synchronous motor drive. Based on theoretical analysis, a loss minimization condition that determines the optimal q-axis component of the armature current was derived. Selected experimental results were presented to validate the effectiveness of the proposed control method.

In 2004, Jian-Xin, X., Panda, S. K., Ya-Jun, P., Tong Heng, L. and Lam, B. H. [14] applied a modular control approach to a interior permanent-magnet synchronous motor (IPMSM) speed control. Based on the functioning of the individual module, the modular approach enabled the powerfully intelligent and robust control modules to easily replace any existing module which did not perform well, meanwhile retaining other existing modules which were still effective. Property analysis was first conducted for the existing function modules in a conventional PMSM control system: proportional-integral (PI) speed control module, reference current-generating module, and PI current control module. The proposed control system was evaluated through real-time implementation and experimental results validated the effectiveness.

Onoda, S. and Emadi, A. in 2004 [15], had developed a modeling tool to study automotive systems using the power electronics simulator (PSIM) software. PSIM was originally made for simulating power electronic converters and motor drives. This user-friendly simulation package was able to simulate electric/electronic circuits.

Venkaterama, G. [16], had developed a simulation for interior permanent magnet motors using GA. The motor was a 5 hp IPM synchronous line start type. Its model included the damper windings required to start the motor and the mathematical model was derived in rotor reference frame. The simulation was presented with the plots of rotor currents, stator currents, speed and torque.

Simulink PM Synchronous Motor Drive demo circuit (2005) [17] used the AC6 block of SimPowerSystems library. It modeled a interior permanent magnet synchronous motor drive with a braking chopper. The speed control loop used a PI regulator to produce the flux and torque references for the vector control block. The vector control block computed the three reference motor line currents corresponding to the flux and torque references and then fed the motor with these currents using a three-phase current regulator. Motor current, speed, and torque

signals were available at the output of the block.

In the above works, none of them have considered a real drive system simulation in Simulink operating at constant torque and flux weakening regions.

1.4 Outline of the Present Work

The thesis is divided into 6 chapters. Chapter II presents a theoretical review of IPM motors drives which deals with the description of the different components of interior permanent magnet motors drive system. A review of permanent magnet materials and classification of permanent magnet motors is also given. Finally a comparison of Interior Permanent Magnet Motors over other ac motors is presented in brief.

Chapter III deals with the detailed modeling of IPMSM, closed loop control techniques used for IPM motor drives, the design of speed control for IPM motor, details about Genetic Algorithm, 4S3P inverter, PI controller.

Chapter IV is deals with the preliminary ideas of artificial neural network and correlated real time recurrent learning algorithm for the recurrent neural network are discussed here. Neural network based stator flux and rotor position estimation technique and the proposed control scheme are also presented in this chapter.

Chapter V deals with the simulation results. Simulation model of the interior permanent magnet synchronous motor is deduced and results of simulation for different operating conditions are shown. At the first stage, the performance of the flux and position estimator is investigated. Then the starting performances of the motor are illustrated under transient and steady- state conditions. Finally, robustness of the control scheme is examined to load fluctuations, speed variation, and parameter perturbation, etc and last the compares between natural algorithm and genetic algorithm.

Finally, Chapter VI presents general conclusions and recommendations for future work.

CHAPTER II

Fundamentals of Interior Permanent Magnet Motor Drive System

2.1 Introduction

The Interior Permanent Magnet Motor is a motor that uses permanent magnets to produce the air gap magnetic field rather than using electromagnets. These motors have significant advantages, attracting the interest of the researchers and industry for use in many applications. This chapter deals with the description of the different components of interior permanent magnet motors drive system. A review of permanent magnet materials and classification of permanent magnet motors is also given. Finally a comparison of Interior Permanent Magnet Motors over other ac motors is presented in brief.

2.2 Interior Permanent Magnet Synchronous Motor Drive System

The motor drive consists of four main components, the IPM motor, inverter, control unit and the position sensor. The components are connected as shown in figure 2.1.

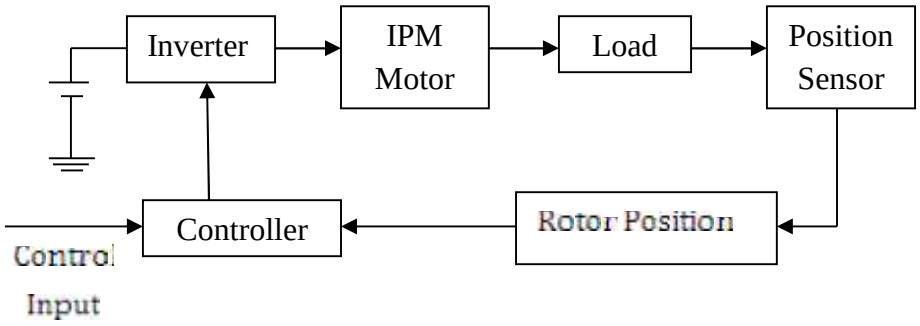

Figure 2.1 Drive System Schematic

An interior permanent magnet synchronous motor (IPMSM) is a motor that uses permanent magnets to produce the air gap magnetic field rather than using electromagnets. These motors have significant advantages, attracting the interest of researchers and industry for use in many applications.

2.2.1 Interior Permanent Magnet Materials

The properties of the interior permanent magnet material will affect directly the performance of the motor and proper knowledge is required for the selection of the materials and for understanding IPM motors.

The earliest manufactured magnet materials were hardened steel. Magnets made from steel were easily magnetized. However, they could hold very low energy and it was easy to demagnetize. In recent years other magnet materials such as Aluminum Nickel and Cobalt alloys (ALNICO), Strontium Ferrite or Barium Ferrite (Ferrite), Samarium Cobalt (First generation rare earth magnet) (SmCo) and Neodymium Iron-Boron (Second generation rare earth magnet) (NdFeB) have been developed and used for making interior permanent magnets.

The rare earth magnets are categorized into two classes: Samarium Cobalt (SmCo) magnets and Neodymium Iron Boride (NdFeB) magnets. SmCo magnets have higher flux density levels but they are very expensive. NdFeB magnets are the most common rare earth magnets used in motors these days. A flux density versus magnetizing field for these magnets is illustrated in figure 2.2.

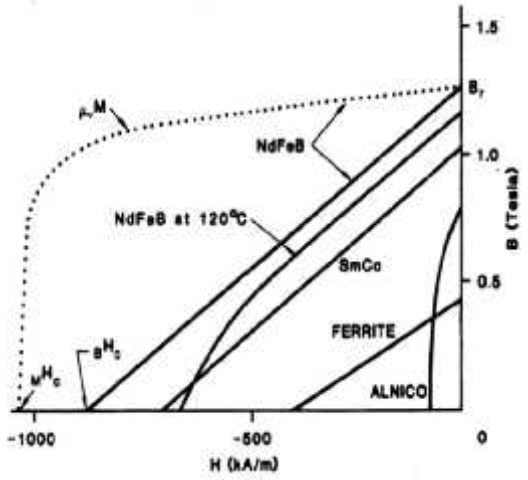

Figure 2.2 Flux Density versus Magnetizing Field of interior Permanent Magnetic Materials

2.2.2 Classification of Interior Permanent Magnet Motors

2.2.2.1 Direction of field flux

IPM motors are broadly classified by the direction of the field flux. The first field flux classification is radial field motor meaning that the flux is along the radius of the motor. The second is axial field motor meaning that the flux is perpendicular to the radius of the motor. Radial field flux is most commonly used in motors and axial field flux have become a topic of interest for study and used in a few applications.

2.2.2.2 Flux density distribution

IPM motors are classified on the basis of the flux density distribution and the shape of current excitation. They are IPMSM and IPM brushless motors (BLDC). The IPMSM has a sinusoidal-shaped back EMF and is designed to develop sinusoidal back EMF waveforms. They have the following:

1. Sinusoidal distribution of magnet flux in the air gap
2. Sinusoidal current waveforms
3. Sinusoidal distribution of stator conductors.

BLDC has a trapezoidal-shaped back EMF and is designed to develop trapezoidal back EMF waveforms. They have the following:

1. Rectangular distribution of magnet flux in the air gap
2. Rectangular current waveform
3. Concentrated stator windings.

2.2.2.3 Interior Permanent Magnet radial field motors

In IPM motors, the magnets can be placed in two different ways on the rotor. Depending on the placement they are called either as surface permanent magnet motor or interior permanent magnet motor.

Surface mounted PM motors have a surface mounted permanent magnet rotor. Each of the PM is mounted on the surface of the rotor, making it easy to build, and specially skewed poles are easily magnetized on this surface mounted type to minimize cogging torque. This configuration is used for low speed applications because of the limitation that the magnets will fly apart during high-speed operations. These motors are considered to have small saliency, thus having practically equal inductances in both axes [18]. The permeability of the permanent magnet is almost that of the air, thus the magnetic material becoming an extension of the air gap. For a surface permanent magnet motor $L_d = L_q$ [19].

The rotor has an iron core that may be solid or may be made of punched laminations for simplicity in manufacturing [20]. Thin permanent magnets are mounted on the surface of this core using adhesives. Alternating magnets of the opposite magnetization direction produce radially directed flux density across the air gap. This flux density then reacts with currents in windings placed in slots on the inner surface of the stator to produce torque. Figure 2.3 shows the placement of the magnet [21].

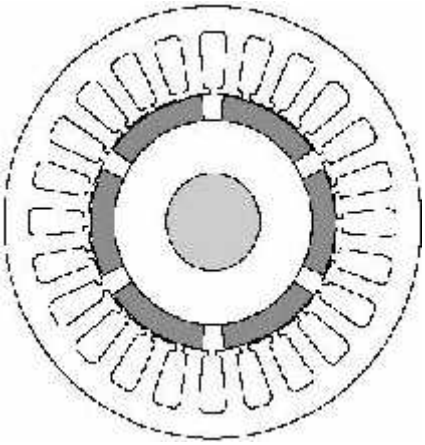

Figure 2.3 Surface Permanent Magnet Motor

Interior PM Motors have interior mounted permanent magnet rotor as shown in figure 2.4. Each permanent magnet is mounted inside the rotor. It is not as common as the surface-mounted type but it is a good candidate for high-speed operation. There is inductance variation for this type of rotor because the permanent magnet part is equivalent to air in the magnetic circuit calculation. These motors are considered to have saliency with q axis inductance greater than the d axis inductance (Lq > L_d) [19].

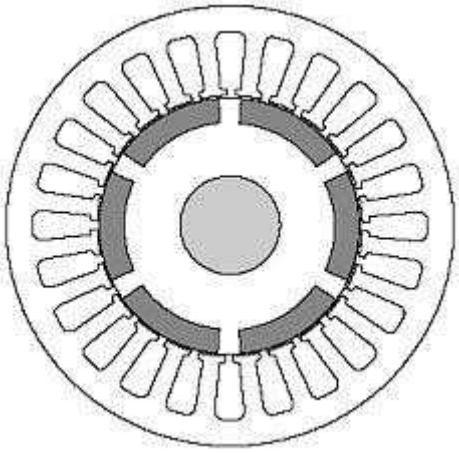

Figure 2.4 Interior Permanent Magnet Motor

2.4 Comparative Study of AC Drives

Recent availability of high energy- density IPM materials at competitive prices, continuing breakthroughs and reduction in cost of powerful fast Digital Signal Processors(DSPs) and micro-controllers combined with the remarkable advances in semiconductor switches and modern control technologies have opened up new possibilities for interior permanent magnet motor drives in order to meet competitive worldwide market demands [22].

The popularity of IPMSMs comes from their desirable features [23]:

- High efficiency
- High torque to inertia ratio
- High torque to volume ratio
- High air gap flux density
- High power factor
- High acceleration and deceleration rates
- Lower maintenance cost
- Simplicity and ruggedness
- Compact structure
- Linear response in the effective input voltage

However, the higher initial cost, operating temperature limitations, and danger of demagnetization mainly due to the presence of presence of interior permanent magnets can be restrictive for some applications.

The main advantages of using interior permanent magnets over field excitation circuit used by conventional synchronous motors are given below [23]:

- Elimination of slip- rings and extra DC voltage supply.
- No rotor copper losses generated in the field windings of wound- field synchronous motor.
- Higher efficiency because of lesser losses.
- Since there is no circuit creating heat on the rotor, cooling of the motor just through the stator in which the copper and iron loses are observed is more easily achieved.
- Reduction of machine size because of high efficiency.
- Different size and different arrangements of permanent magnets on the rotor will lead to have wide variety of machine characteristics.

IPMAC motors have gained more popularity especially after the advent of high performance rare- earth permanent magnets, like samarium cobalt and neodymium- boron iron which surpass the conventional material in DC brush and are becoming more and more attractive for industrial applications.

The positive specific characteristics of IPMAC motors explained above make them highly attractive candidates for several classes of drive applications, such as in servo- drives containing motors with allow to mid power range, robotic applications, motion control system, aerospace actuators, low integral- hp industrial drives, fiber spinning and so on. Also high power rating IPMAC motors have been built, for example, for ship propulsion drives up to 1 MW. Recently two major sectors of consumer market are starting to pay more attention to the IPM motor drive due to its features.

IPMAC motors have many advantages over DC brush motors and IMs. Most of these are summarized as [22]:

- High dynamic response
- High efficiency providing reduction in machine size
- Long operating life
- Noiseless operation
- High power factor
- High power to weight ratio; considered the best comparing to other available electric motors
- High torque to inertia ratio; providing quick acceleration and deceleration for short time
- High torque to volume ratio
- High air- gap flux density
- Higher speed ranges

- Better speed verses torque characteristic
- Lower maintenance cost
- Simplicity and ruggedness
- Compact design
- Linear response
- Controlled torque at zero speed

Compared to IMs, IPMSMs have some advantages, such as higher efficiency in steady- state, and operate constantly at synchronous speed. They do not have losses due to the slip which occurs when the rotor rotates at a slightly slower speed than the stator because the process of electromagnetic induction requires relative motion called “slip” between the rotor conductors and the stator rotating field that is special to IM operation. The slip makes the IM asynchronous, meaning that the rotor speed is no longer exactly proportional to the supply frequency [22].

2.5 Conclusion

A detailed discussion on the interior permanent magnet motor is presented in this chapter. The properties of magnetic materials directly affect the performance of the interior permanent magnet motors. Therefore, brief descriptions on the commercially available magnetic materials are presented here. A classification of interior permanent magnet motors depending on various characteristics is included also. The advantages of interior permanent magnet motors over induction motors, DC brush motors, etc in various aspects is also presented. The above discussion proves the superiority of the interior permanent magnet synchronous motor for industry applications.

CHAPTER III

Analysis of Interior Permanent Magnet Synchronous Motor (IPMSM)

3.1 Introduction

This chapter provides a summary literature review for the design and analysis of new IPMSM. An IPMSM is widely used for a high-power and high-speed application. Since the study of an IPMSM is relatively new technology compared to DC motor and induction motor, there are many research areas which are not still fully developed.

One of the areas to solve is extending the speed limit which is one of the drawbacks of an IPMSM. This chapter provides an explanation of mathematical model of IPMSM, Genetic Algorithm, PI controller, mathematical model of 4S3P which parameters cause the speed limit, and how to calculate these parameters.

3.2 Mathematical Model of IPMSM

The IPMSM is similar to the conventional wire- wound excited synchronous motor with the exception is provided by the permanent magnets instead of a wire- would dc motor field. Therefore, the d-q axis model of the IPMSM can be derived from the standard model for synchronous machines by removing the equation related to the field current and associated dynamics. The flux linkages in the three- stator phase windings due to the permanent magnets of the rotor are given in matrix form as [24]:

$$\begin{bmatrix}\psi_a\\ \psi_b\\ \psi_c\end{bmatrix} = \psi_m \begin{bmatrix}\sin\theta_r\\ \sin(\theta_r - \frac{2\pi}{3})\\ \sin(\theta_r + \frac{2\pi}{3})\end{bmatrix} \quad 3.1$$

Where ψ_a , ψ_b and ψ_c are the a, b and c phase stator flux linkages due to permanent magnet alone, respectively, ψ_m is the constant flux supplied by the permanent magnets and θ_r is the rotor position angle.

The three- phase air gap flux linkage equations are given in matrix form as:

$$\begin{bmatrix}\psi_a\\ \psi_b\\ \psi_c\end{bmatrix} = \begin{bmatrix}L_a & M_a & M_a\\ M_b & L_b & M_b\\ M_c & M_c & L_c\end{bmatrix}\begin{bmatrix}i_a\\ i_b\\ i_c\end{bmatrix} + \psi_m \begin{bmatrix}\sin\theta_r\\ \sin(\theta_r - \frac{2\pi}{3})\\ \sin(\theta_r + \frac{2\pi}{3})\end{bmatrix} \quad 3.2$$

Where ψ_a, ψ_b and ψ_c are the three- phase air gap flux linkage, L_a , L_b , L_c are the self inductances and M_a , M_b , M_c are the mutual inductances.

Now, the voltage equations of the three phases of the IPMSM can be defined as:

$$v_a = r_a i_a + \frac{d\psi_a}{d} \quad 3.3$$

$$v_b = r_b i_b + \frac{d\psi_b}{d} \quad 3.4$$

$$v_c = r_c i_c + \frac{d\psi_c}{d} \quad 3.5$$

Where v_a, v_b, v_c are the three- phase voltages, i_a, i_b, i_c are the three- phase currents and r_a, r_b, r_c are the three- phase stator resistances.
In matrix form Equation (3.5) can be written as,

$$\begin{bmatrix} V_a \\ V_b \\ V_c \end{bmatrix} = \begin{bmatrix} r_a & 0 & 0 \\ 0 & r_b & 0 \\ 0 & 0 & r_c \end{bmatrix} \begin{bmatrix} i_a \\ i_b \\ i_c \end{bmatrix} + p \begin{bmatrix} \psi_a \\ \psi_b \\ \psi_c \end{bmatrix} \quad 2.6$$

Where p is the differential operator, $\frac{d}{d}$. Equations (3.2) indicate that the flux linkages as well as the machine inductances are functions of rotor position and hence function of rotor speed. Therefore, the coefficients of the voltages are time varying except when the motor is stationary. In order to avoid the complexity of calculations, all the equations have to be transformed to the synchronously rotating rotor reference frame where the machine equations are no longer dependent on the rotor position. These transformations can be accomplished in two steps using the Park transformation equations [24]. In the first step, the machine equations are to be transformed from the stationary a-b-c frame into the stationary d-q frame and in the second step, from the stationary d-q frame to the synchronously rotating $d^r - q^r$ frame. The phase variables in terms of d-q variables can be written in matrix form as,

$$\begin{bmatrix} x_a \\ x_b \\ x_c \end{bmatrix} = \begin{bmatrix} \cos\theta_r & \sin\theta_r & 1 \\ \cos(\theta_r - \frac{2\pi}{3}) & \sin(\theta_r - \frac{2\pi}{3}) & 1 \\ \cos(\theta_r + \frac{2\pi}{3}) & \sin(\theta_r + \frac{2\pi}{3}) & 1 \end{bmatrix} \begin{bmatrix} x_q \\ x_d \\ x_0 \end{bmatrix} \quad 3.7$$

Wherex_a, x_b and x_c are the a, b and c phase quantities, respectively, x_d, x_q and x_0 are the d- axis, q- axis and zero sequence components, respectively. The matrix element x may represent either voltage or current.

Equation (3.7) can be written in compact form as,

$$[X_a \quad] = [C]^{-1}[X_q \quad] \quad 3.8$$

Where C is the coefficient matrix.

The corresponding inverse relation can be written as,

$$\begin{bmatrix} x_q \\ x_d \\ x_0 \end{bmatrix} = \frac{2}{3}\begin{bmatrix} \cos\theta_r & \cos(\theta_r - \frac{2\pi}{3}) & \cos(\theta_r + \frac{2\pi}{3}) \\ \sin\theta_r & \sin(\theta_r - \frac{2\pi}{3}) & \sin(\theta_r + \frac{2\pi}{3}) \\ \frac{1}{2} & \frac{1}{2} & \frac{1}{2} \end{bmatrix}\begin{bmatrix} x_a \\ x_b \\ x_c \end{bmatrix} \quad 3.9$$

or in compact form as,

$$[X_{qd0}] = [C][X_{abc}] \quad 3.10$$

The rotor position angle θ_r is defined as,

$$\theta_r = \int_0^t \omega_r(t)dt + \theta_r(0) \quad 3.11$$

Equations (3.7) and (3.9) are both in a stationary reference frame, so θ_r is only the initial rotor position, $\theta_r(0)$, which is also the angle difference between the q- axis and a- phase. For balanced 3- phase, x_0 does not exist, and it is also convenient to set $\theta_r(0) = 0$ so that the q- axis coincides with a- phase. Under these conditions equations (3.7) and 3.9) can be written, respectively, as

$$\begin{bmatrix} x_a \\ x_b \\ x_c \end{bmatrix} = \begin{bmatrix} 1 & 0 \\ \frac{-1}{2} & \frac{-\sqrt{3}}{2} \\ \frac{-1}{2} & \frac{\sqrt{3}}{2} \end{bmatrix}\begin{bmatrix} x_q \\ x_d \end{bmatrix} \quad 3.12$$

And $$\begin{bmatrix} x_q \\ x_d \end{bmatrix} = \begin{bmatrix} \frac{2}{3} & \frac{-1}{3} & \frac{-1}{3} \\ 0 & \frac{-1}{\sqrt{3}} & \frac{1}{\sqrt{3}} \end{bmatrix}\begin{bmatrix} x_a \\ x_b \\ x_c \end{bmatrix} \quad 3.13$$

The relative position of the stationary d-q axis and the rotating $d^r - q^r$ axis is shown in Fig. 3.1. Now the quantities in the stationary d-q frame can be converted to the synchronously rotating $d^r - q^r$ frame with the help of Fig. 3.1 as:

$$\begin{bmatrix} x_q^r \\ x_d^r \end{bmatrix} = \begin{bmatrix} \cos\theta_r & -\sin\theta_r \\ \sin\theta_r & \cos\theta_r \end{bmatrix}\begin{bmatrix} x_q \\ x_d \end{bmatrix} \quad 3.14$$

The inverse relation can be written as,

$$\begin{bmatrix} x_q \\ x_d \end{bmatrix} = \begin{bmatrix} \cos\theta_r & \sin\theta_r \\ -\sin\theta_r & \cos\theta_r \end{bmatrix}\begin{bmatrix} x_q^r \\ x_d^r \end{bmatrix} \quad 3.15$$

In order to derive the $d^r - q^r$ model of the IPMSM drive, the following assumptions are made:
(a) The eddy current and hysteresis losses are negligible.
(b) The induced emf is sinusoidal.
(c) The saturation is neglected.
(d) The stator resistances of the three phases are balanced.

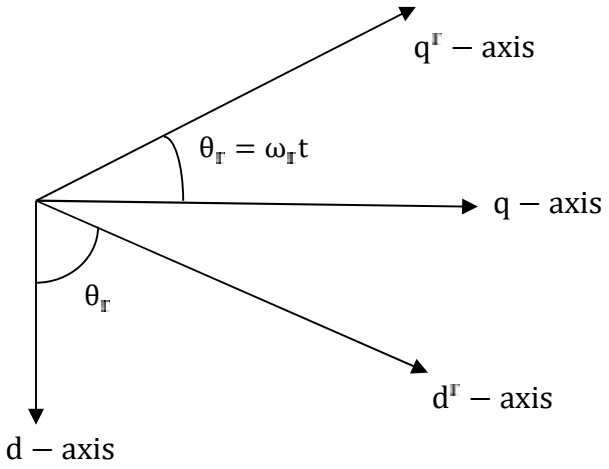

Fig. 3.1 Relative positions of stationary d − q axes and rotating $d^r - q^r$ axes.

With the above assumptions and using Equations (3.6), (3.7) and (3.15), the $d^r - q^r$ axis model of the IPMSM can be written as,

$$v_q^r = r_s i_q^r + p\psi_q^r + \omega_s \psi_d^r \quad 3.16$$

$$v_d^r = r_s i_d^r + p\psi_d^r + \omega_s \psi_q^r \quad 3.17$$

Where v_d^r and v_q^r are d and q axis voltages i_d^r and i_q^r are d and q axis currents, ψ_d^r and ψ_q^r are d and q axis flux linkages, respectively, r_s is the stator resistance per phase and ω_s is the stator frequency.
ψ_d^r and ψ_q^r can be written as,

$$\psi_q^r = L_q i_q^r \quad 3.18$$

$$\psi_d^r = L_d i_d^r + \psi_m \quad 3.19$$

Where,

$$L_q = L_l + L_m \quad 3.20$$

$$L_d = L_l + L_m \quad 3.21$$

L_d and L_q are d and q axis inductances, L_m and L_m are d and q axis magnetizing inductances and L_l is the leakage inductance per phase. The stator frequency ω_s is related to the rotor frequency ω_r as,

$$\omega_s = P\omega_r \tag{3.22}$$

Where P is the number of pole- pairs. Therefore, Equations (3.16) and (3.17) can be rewritten as,

$$\begin{bmatrix} v_q^r \\ v_d^r \end{bmatrix} = \begin{bmatrix} r_s + pL_q & P\omega_r L_d \\ -P\omega_r L_q & r_s + pL_d \end{bmatrix} \begin{bmatrix} i_q^r \\ i_d^r \end{bmatrix} + \begin{bmatrix} P\omega_r \psi_m \\ 0 \end{bmatrix} \tag{3.23}$$

According to Equation (3.23), the permanent magnet synchronous motor can be represented by the d^r and q^r axis equivalent circuit diagrams as shown in Fig. 3.2. The torque developed by the machine can be obtained by considering the power entering the two sources as shown in Fig. 3.2. The permanent magnet is represented as a current source,I_m, [25] in Fig. 3.2(a).

The total average power entering the sources which is also the developed power per phase is given by,

$$P_p = (-P\omega_r L_q i_q^r i_d^r + P\omega_r L_d i_d^r i_q^r + P\omega_r \psi_m i_q^r)(\frac{1}{2}) \tag{3.24}$$

Therefore, the total power developed by the machine is,

$$P_m = \frac{3}{2}\frac{\omega_r}{2}\{\psi_m i_q^r + (L_d - L_q) i_d^r i_q^r\} \tag{3.25}$$

Now the electromagnetic torque is given by,

$$T_e = \frac{P_m}{\omega_r} = \frac{3}{2}[\psi_m i_q^r + (L_d - L_q) i_d^r i_q^r] \tag{3.26}$$

The motor dynamics can be represented by the following equation:

$$T_e = T_L + B_m\omega_r + J_m p\omega_r \tag{3.27}$$

Where T_L is the load torque (in Nm), B_m is the friction damping coefficient (in Nm/rad. /sec.) and J_m is the rotor inertia constant (in kg- m^2).

For dynamic simulation the IPMSM model equations may be expressed as follows:

$$Pi_q^r = (V_q^r - Ri_q^r - P\omega_r L_d i_d^r - P\omega_r \psi_m)/L_q \tag{3.28}$$

$$Pi_d^r = (V_d^r - Ri_d^r - P\omega_r L_q i_q^r)/L_d \tag{3.29}$$

$$P\omega_r = (T_e - T_L - B_m\omega_r)/J_m \tag{3.30}$$

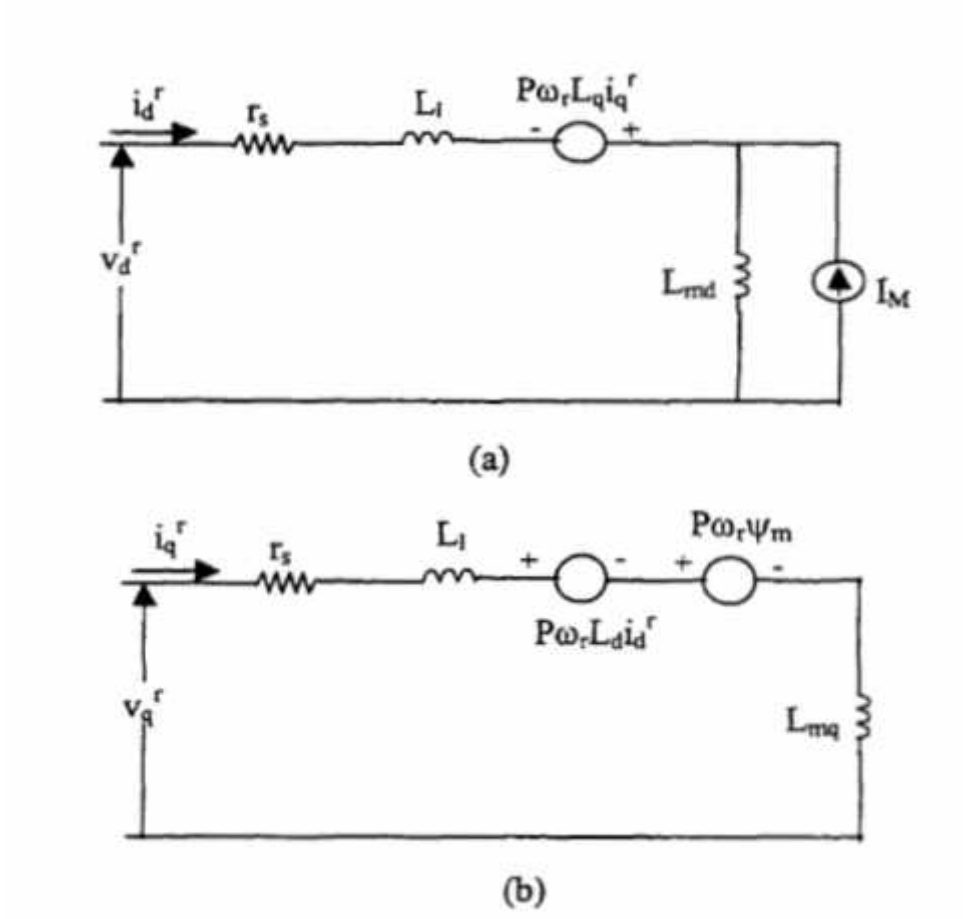

Fig. 3.2. Equivalent circuit model of the IPMSM: (a) d − axis, (b) q − Axis.

The motor parameters used in the simulation are given in Appendix A.

3.3 Vector Control Strategy for IPMSM Drive

The vector control technique is one of the most effective techniques for use with ac motors in high performance drives. The IPMSM can be vector controlled when the machine equations are transformed from the a-b-c frame to the synchronously rotating $d^r - q^r$ frame where the sinusoidal quantities become constant. In the case of dc motor control, the developed torque T_e can be expressed as,

$$T_e = K_t' I_a \psi_f = K_t I_a I_f \qquad 3.31$$

Where K_t', K_t are constants, I_a is the armature current, I_f is the field current and ψ_f is the field flux linkage. Both I_a and I_f are orthogonal and decoupled vectors. Hence the control task

becomes much easier for the separately excited dc motor. In the case of the interior permanent magnet synchronous motor (PMSM), the torque Equation (3.26) has two terms:

The first term represents the magnet torque produced by the interior permanent magnet flux ψ_m and the torque producing current component i_q^r.
The second term represents the reluctance torque produced by the complex interaction of inductances L_d and L_q and also the current i_d^r and i_q^r. In the case of the surface mounted permanent magnet synchronous motor, $L_d \cong L_q$ so the contribution of the second term in Equation (3.26) is negligible.

Therefore, the torque equation of the surface mounted permanent magnet synchronous motor becomes linear and hence the control task is easier. However, in the case of the interior permanent magnet synchronous motor (IPMSM), L_d is larger thanL_q. Moreover, it is also known that the excitation voltage due to permanent magnets, and the values of the inductances L_d and L_q undergo significant variations in an interior type permanent magnet motor under different steady state and dynamic loading conditions [26]. Thus, the complexity of the control of the IPMSM drive arises due to the nonlinear nature of the torque Equation (3.26). In order to operate the motor in a vector control scheme avoiding the complexity i_d^r is set to zero. Then the torque equation becomes linear and is given by,

$$T_e = \frac{3}{2}\psi_m i_q^r = K\psi_m i_q^r \qquad 3.32$$

Where the constant $K = \frac{3}{2}$. It is to be noted that the torque expressions of the Equations (3.31) and (3.32) are identical and decoupled. Using phasor diagrams notations and taking the d^r axis as a reference phasor, the steady state phase voltage V_a can be derived from the steady state $d^r - q^r$axis voltage Equation (3.23) as,

$$V_a = v_d^r + jv_q^r$$
$$= r_s I_a - \omega_s L_q i_q^r + j\omega_s L_d i_d^r + j\omega_s \psi_m \qquad 3.33$$

Where the phase current, $I_a = -i_d^r + ji_q^r$ 3.34

In case of the IPM motor, the d^r- axis current is negative and it demagnetizes the main flux provided by the permanent magnets. Thus, in order to take only the absolute value of i_d^r we can re-write the Equation (3.33) as follows:

$$V_a = r_s I_a - \omega_s L_q i_q^r - j\omega_s L_d i_d^r + j\omega_s \psi_m \qquad 3.35$$

According to Equation (3.33) the basic vector diagram of IPMSM is shown in Fig. 3.3(a). The vector control scheme can be clearly understood by this vector diagram. It is shown in the vector diagram that the stator current can be controlled by controlling the d^r and q^r axis current components. In the vector control scheme, when i_d^r is set to zero then all then flux linkages are

oriented in the d^r-axis as shown in Fig. 3.3(b). After setting $i_d^r = 0$, Equation (3.32) shows that the torque is a function of only the quadrature axis current component, and hence a constant torque can be obtained by ensuring i_q^r constant. With the $i_d^r = 0$ control technique, the dynamic Equations (3.28) to (3.30) of IPMSM can be rewritten as,

$$pi_q^r = v_q^r - Ri_q^r - K_b\omega_r)/L_q \quad 3.36$$

$$v_d^r = -P\omega_r L_q I_q^r \quad 3.37$$

$$p\omega_r = K_T i_q^r - T_L - B_m\omega_m)/J_m \quad 3.38$$

Where $K_T = (3/2)K_b$ and $K_b = P\psi_m$.

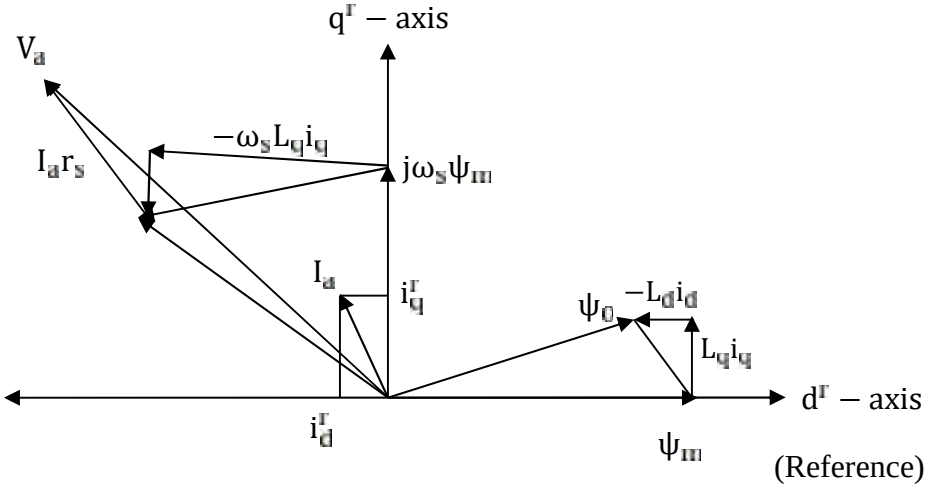

(a)

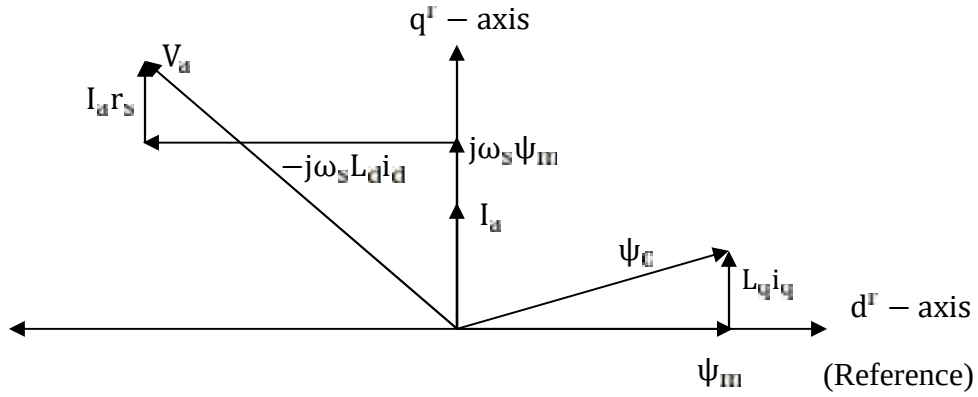

(b)

Fig. 3.3 Basic vector diagram of IPMSM: (a) general: (b) modified with $i_d = 0$

3.4 Parks Transformation and Dynamic d-q Modeling

The dynamic d-q modeling is used for the study of motor during transient and steady state. It is done by converting the three phase voltages and currents to dq0 variables by using Parks Transformation [27].

Converting the phase voltages variables V_a to V_d variables in rotor reference frame the following equations are obtained

$$\begin{bmatrix} V_q \\ V_d \\ V_0 \end{bmatrix} = \frac{2}{3}\begin{bmatrix} \cos\theta_r & \cos(\theta_r - 120) & \cos(\theta_r + 120) \\ \sin\theta_r & \sin(\theta_r - 120) & \sin(\theta_r + 120) \\ 1/2 & 1/2 & 1/2 \end{bmatrix}\begin{bmatrix} V_a \\ V_b \\ V_c \end{bmatrix} \quad 3.39$$

Convert V_d to V_a

$$\begin{bmatrix} V_a \\ V_b \\ V_c \end{bmatrix} = \begin{bmatrix} \cos\theta_r & \sin\theta_r & 1 \\ \cos(\theta_r - 120) & \sin(\theta_r - 120) & 1 \\ \cos(\theta_r + 120) & \sin(\theta_r + 120) & 1 \end{bmatrix}\begin{bmatrix} V_q \\ V_d \\ V_0 \end{bmatrix} \quad 3.40$$

3.5 IPM Motor Control

Control of IPM motors is performed using field oriented control for the operation of synchronous motor as a dc motor. The stator windings of the motor are fed by an inverter that generates a variable frequency variable voltage. Instead of controlling the inverter frequency independently, the frequency and phase of the output wave are controlled using a position sensor as shown in figure 3.4

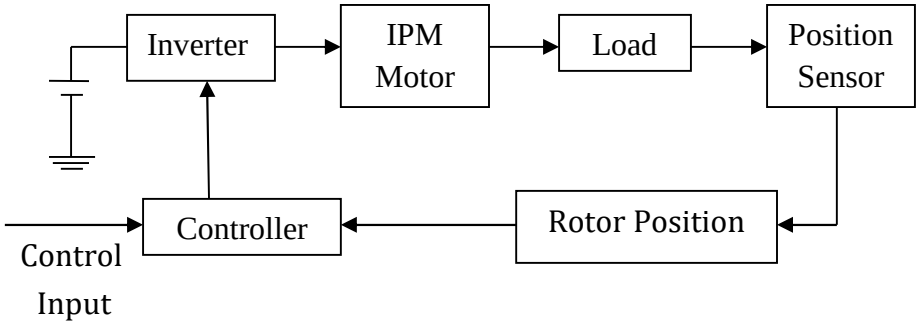

Fig. 3.4 Self control synchronous motor

Field oriented control was invented in the beginning of 1970s and it demonstrates that an induction motor or synchronous motor could be controlled like a separately excited dc motor by the orientation of the stator mmf or current vector in relation to the rotor flux to achieve a desired objective. In order for the motor to behave like DC motor, the control needs knowledge of the position of the instantaneous rotor flux or rotor position of permanent magnet motor. This needs a resolver or an absolute optical encoder. Knowing the position, the three phase currents can be

calculated. Its calculation using the current matrix depends on the control desired. Some control options are constant torque and flux weakening. These options are based in the physical limitation of the motor and the inverter. The limit is established by the rated speed of the motor, at which speed the constant torque operation finishes and the flux weakening starts as shown in figure 3.5.

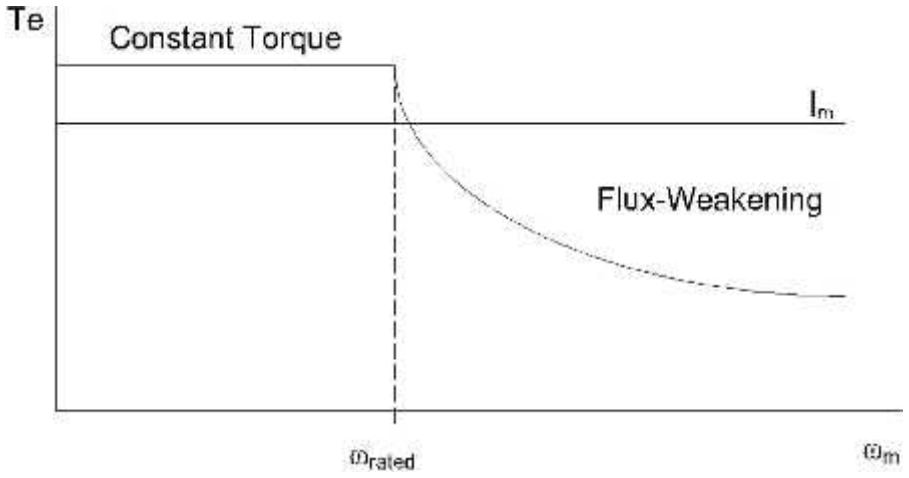

Figure 3.5 Steady State Torque versus Speed

3.6 Field Oriented Control of IPM Motors

The IPMSM control is equivalent to that of the dc motor by a decoupling control known as field oriented control or vector control. The vector control separates the torque component of current and flux channels in the motor through its stator excitation.

The vector control of the IPM synchronous motor is derived from its dynamic model. Considering the currents as inputs, the three currents are:

$$i_a = I_m \sin(\omega_r t + \alpha) \quad 3.41$$

$$i_b = I_m \sin(\omega_r t + \alpha - \frac{2\pi}{3}) \quad 3.42$$

$$i_c = I_m \sin(\omega_r t + \alpha + \frac{2\pi}{3}) \quad 3.43$$

$$\begin{bmatrix} i_a \\ i_b \\ i_c \end{bmatrix} = \begin{bmatrix} \cos(\omega_r t + \alpha) \\ \cos(\omega_r t + \alpha - \frac{2\pi}{3}) \\ \cos(\omega_r t + \alpha + \frac{2\pi}{3}) \end{bmatrix} [I_m] \quad 3.44$$

Where α is the angle between the rotor field and stator current phasor, ω_r is the electrical rotor speed.

3.7 Genetic Algorithm (GA)

GA is a stochastic global adaptive search optimization technique based on the mechanisms of natural selection [28]. GA was first suggested by John Holland and his colleagues in 1975. GA has been recognized as an effective and efficient technique to solve optimization problems. Compared with other optimization techniques, such as simulating annealing and random search method techniques, GA is superior in avoiding local minima, which is a significant issue in the case of nonlinear systems [29]. GA starts with an initial population containing a number of chromosomes where each one represents a solution of the problem, the performance of which is evaluated by a fitness function.

Basically, GA consists of three main stages: Selection, Crossover and Mutation. The application of these three basic operations allows the creation of new individuals, which may be better than their parents. This algorithm is repeated for many generations and finally stops when reaching individuals that represent the optimum solution to the problem. The GA architecture is shown in Fig. 3.6 [28, 30].

In each generation, the genetic operators are applied to selected individuals from the current population in order to create a new population. Generally, the three main genetic operators of reproduction, crossover and mutation are employed.

By using different probabilities for applying these operators, the speed of convergence can be controlled. Crossover and mutation operators must be carefully designed, since their choice greatly contributes to the performance of the whole genetic algorithm [31].

Producing initial populations is the first step of GA. The population is composed of the chromosomes that are binary bit stream or real codes. The corresponding evaluation of a population is called the fitness function. It is the performance index of a population. In this project the fitness function is defined as

$$F = (\omega_{r} - \omega_{r})^{2} \qquad 3.45$$

The evolution of CGA is shown in Fig. 3.6. The overshoot and settling time of the controlled system is used as the performance index of fitness function. Then fitness function [32] can be defined as$F = f_1 \times f_2$. The definitions of f_1 and f_2 are$f_1 = e^{-(OT/K_1)^2}$,$f_2 = e^{-(ST/K_2)^2}$, where OT is the overshoot time quantity and ST is the setting time quantity. K_1, K_2 are weight factors that control the value of overshoot and setting time.

After the fitness function is calculated, the fitness value and the number of the generation determine whether the evolution procedure is stopped or not. In the following, the new populations are generated through reproduction, crossover, and mutation.

Reproduction is a process to decide how many copies of individuals strings should be produced in the mating pool according to their allows strings with higher fitness value. The reproduction operation allows strings with higher fitness value to have larger number of population while the strings with lower fitness values have a relatively smaller number of copies or even none at all.

The selection operation decides which parents take part in reproducing offspring for the next generation.

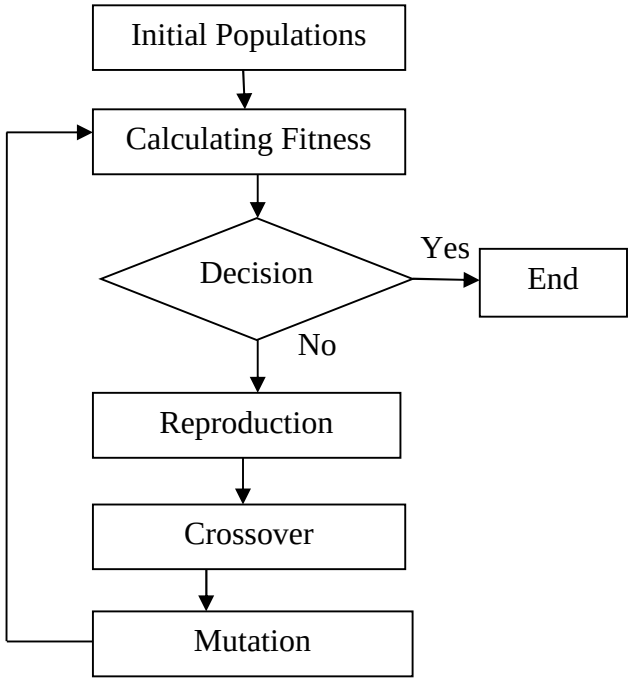

Figure 3.6 Evolution Procedure of GA

Crossover is a recombined operator for two high- fitness strings (parents) to produce two off springs matching their desirable quantities through a random process. The crossover operation is applied to generate new chromosomes. The equations of the new populations generated from crossover are [32]

$$x_o = (1-\alpha)x_p + \alpha x_p \quad 3.46$$

$$x_o = (1-\alpha)x_p + \alpha x_p \quad 3.47$$

Where x_p and x_p are the old chromosomes, α is the random value from 0 to 1, x_o and x_o are the new chromosomes.

Mutation is a method to find the global optimum value. It is a process to provide an occasional random alternation of the value at a particular string position. In the project, Time Variant Mutation (TVM) operator is used to mutate all variables of offspring [32]. It is ought to be taken care that initially this type of mutation might violate the domain of the object variables. In case of domain violations for any offspring, that offspring s left without mutation.

In this project work, Genetic Algorithm is used to optimize the gains of PI controller in the speed loop of the control system for comparing with the performance of the PI based control system. Parameters used in Genetic Algorithm are given bellow:

Population size= 20; Crossover Probability= [0 to 1]. Selected from united random number; Mutation Probability= 0.4; No. of Generation=100.

3.8 Comparative analysis between GA and PI based Synchronous Motor Drive

Fast speed response of synchronous motor is achieved using Genetic Algorithm based PI controller tuning compared with PI controlled tuning and shown in Fig 3.7. It observed that GA based system needs 0.22 sec to speed up the motor at reference speed 1500 rpm where PI based system needs 0.45 sec

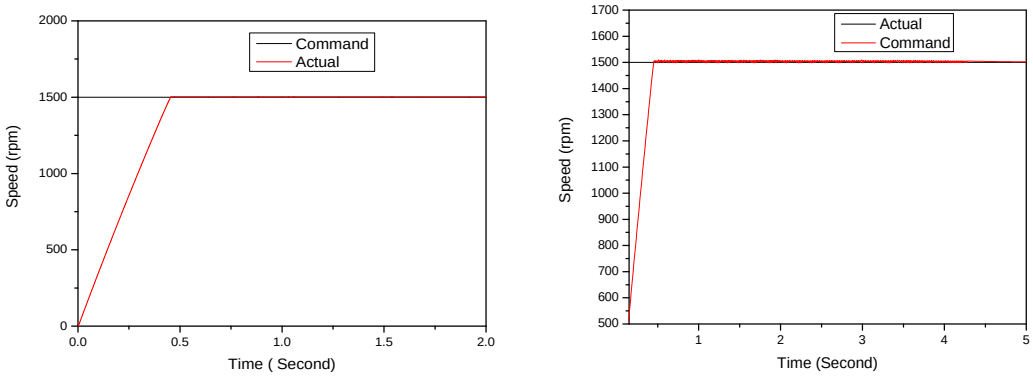

(a) (b)

Figure 3.7(a) Speed response of synchronous drive using PI controller, (b) speed response of synchronous motor drive using GA based PI controller

3.9 Mathematical Model of 4S3P Inverter

The power circuit of the IPMSM fed from 4S3P voltage source inverter is shown in fig.3.8. The circuit consists of two parts; first part is a front- end rectifier powered from single phase supply. The output dc voltage is smoothed through a two series connected capacitors. The second part of the power circuit is the three phase four switch inverter.

The maximum obtainable peak value of the line voltages equals V_d . In the analysis, the inverter switches are considered as ideal switches. The output voltages are defined by the gating signals of the two leg switches and by the two dc link voltages, V_d .

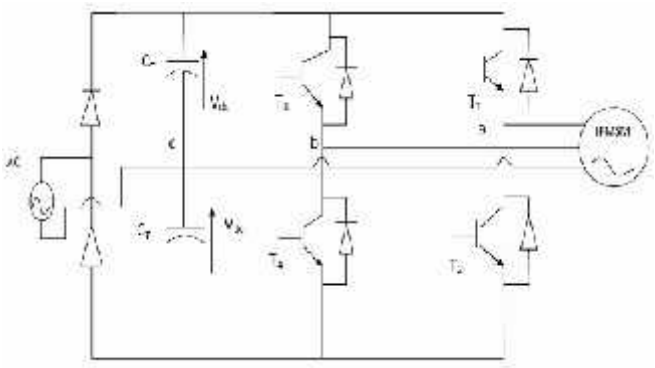

Figure 3.8 IPMSM fed from a four switch inverter.

The phase voltage equations of the motor can be written as a function of the switching logic of the switches and the dc- link voltage V_d [33] by

$$V_a = \frac{V_d}{3}[4S_a - 2S_b - 1] \quad 3.48$$

$$V_b = \frac{V_d}{3}[4S_b - 2S_a - 1] \quad 3.49$$

$$V_c = \frac{V_d}{3}[-2S_a - 2S_b + 2] \quad 3.50$$

Where, V_a, V_b, V_c are inverter output voltages: V_d is voltage across the dc link capacitors; S_a, S_b are switching function for each phase leg.

In matrix form the above equations can be written as

$$\begin{bmatrix} V_a \\ V_b \\ V_c \end{bmatrix} = \frac{V_d}{3}\begin{bmatrix} 4 & -2 \\ -2 & 4 \\ -2 & -2 \end{bmatrix} + \frac{V_d}{3}\begin{bmatrix} -1 \\ -1 \\ 2 \end{bmatrix} \quad 3.51$$

For a balanced capacitor voltages, the four switching combinations lead to four voltage vectors as shown in Fig.3.8 [33]. Table 3.1 shows the different mode of operation and the corresponding output voltage vector of the inverter. Fig. 3.9 shows the waveforms for the 3- phase voltages obtained from the inverter operation.

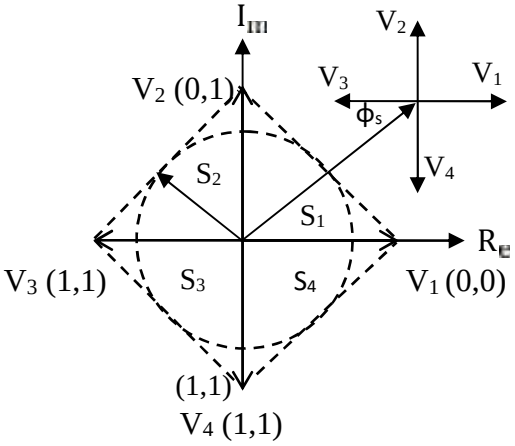

Figure 3.9 Switching vectors for a four switch inverter

Table 3.1
Inverter Model of Operation

Switching function		Switch on		Output voltage vector		
S_a	S_b			V_a	V_b	V_c
0	0	T_2	T_4	$-V_d\ /3$	$-V_d\ /3$	$2V_d\ /3$
0	1	T_2	T_3	$-V_d$	V_d	0
1	0	T_1	T_4	V_d	$-V_d$	0
1	1	T_1	T_3	$V_d\ /3$	$V_d\ /3$	$-2V_d\ /3$

3.10 Controller Models

Automatic control has played a vital role in the advance of engineering and science. An automatic controller compare the actual value of the plant output with the reference input, determine the deviation and produces a control signal that will reduce the derivation to zero or to a small value. The manner in which the automatic controller produces the control signal is called control action.

3.10.1 PI Controller

A PI controller responds to an error signal in a closed control loop and attempts to adjust the controlled quantity to achieve the desired system response. The controlled parameter can be any measurable system quantity such as speed, torque, or flux. The benefit of the PI controller is that it can be adjusted empirically by varying one or more gain values and observing the change in system response. A digital PI controller is executed at a periodic sampling interval. It is assumed that the controller is executed frequently enough so that the system can be properly controlled. The error signal is formed by subtracting the desired setting of the parameter to be controlled from the actual measured value of that parameter. The sign of the error indicates the direction of change required by the control input.

The Proportional (P) term of the controller is formed by multiplying the error signal by a P gain, causing the PI controller to produce a control response that is a function of the error magnitude. As the error signal become larger, the P term of the controller becomes larger to provide more correction. The effect of the P term tends to reduce the overall error as time elapses. However, the effect of the P diminishes as the error approaches zero. In most systems, the error of the controlled parameter gets very close to zero but does not converge. This results in a small remaining steady state error.

The Integral (I) term of the controller is used to eliminate the steady state errors. The I term calculates a continuous running total of the error signal. Therefore, a small steady state error

accumulates into a large error value over time. This accumulated error signal is multiplied by an I gain factor and becomes the I output term of the PI controller.

For a controller with proportional control action, the value of the controller output u(t) is proportional to the actuating error signal e(t). That is,

$$u_p(t) = K_p e(t) \qquad 3.52$$

For a controller with integral action, the value of the controller output u(t) is changed at a rate proportional to the actuating error signal e(t). That is,

$$u_I(t) = K_i \int_0^t e(t)dt \qquad 3.53$$

PI controller combines the function of proportional and integral controllers. So, in case of PI control action, the controlled output will be,

$$u(t) = K_p e(t) + K_i \int_0^t e(t)d \qquad 3.54$$

From (3.52) we get by Laplace transformation

$$\frac{U(s)}{E(s)} = K_p + \frac{K_i}{s} \qquad 3.55$$

The block diagram of a PI controller is shown in Fig. 3.10

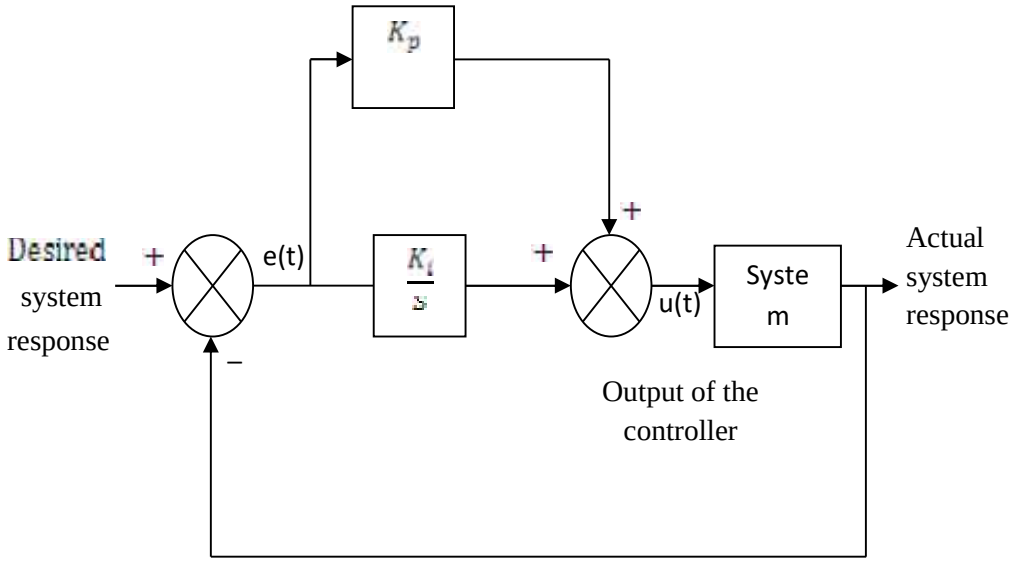

Figure 3.10 Block diagram of a PI controller

3.11 Hysteresis current controller

The hysteresis modulation is a feedback current control method where the motor current tracks the reference current within a hysteresis band. The following figure shows the operation principle of the hysteresis modulation. The controller generates the sinusoidal reference current of desired magnitude and frequency that is compared with the actual motor line current. If the current exceeds the upper limit of the hysteresis band, the upper switch of the inverter arm is turned off and the lower switch is turned on. As a result, the current starts to decay. If the current crosses the lower limit of the hysteresis band, the lower switch of the inverter arm is turned off and the upper switch is turned on. As a result, the current gets back into the hysteresis band. Hence, the actual current is forced to track the reference current within the hysteresis band.

3.11.1 Operation Principle of Hysteresis Modulation

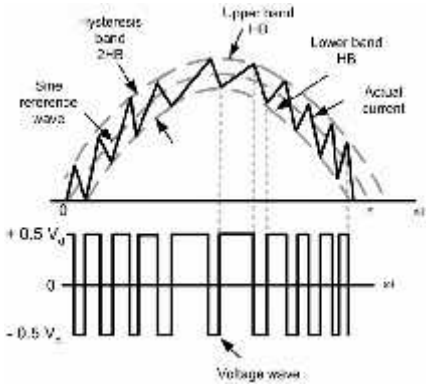

Figure 3.11. Hysteresis current controller

The following figure shows the hysteresis current control modulation scheme, consisting of three hysteresis comparators, one for each phase. This type of closed-loop PWM is used in AC3 and AC5 models.

3.11.2 Typical Hysteresis Current Controller

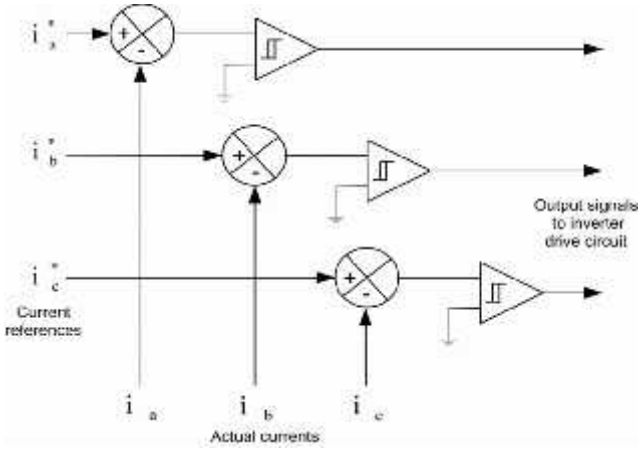

Figure 3.12. Typical Hysteresis Current Controller

The space vector modulation technique differs from the hysteresis modulation in that there are not separate comparators used for each of the three phases. Instead, a reference voltage space vector V_s is produced as a whole, sampled at a fixed frequency, and then constructed through adequate timing of adjacent nonzero inverter voltage space vectors V_1 to V_6 and the zero voltage space vectors V_0, V_7. A simplified diagram of a VSI inverter is shown below. In this diagram, the conduction state of the three legs of the inverter is represented by three logic variables, SA, SB, and SC. A logical 1 means that the upper switch is conducting and logical 0 means that the lower switch is conducting.

3.12 Tuning of the PI Speed Controller Using the Genetic Algorithm Approach

GA can be applied in the tuning of the PI speed controller's gains (K_p, K_i) to ensure optimal control performance at nominal condition for the induction motor.
The block diagram for the entire system is given below:

The objective function used is the following one [34]:

$$\text{Fitness} = \int_0^t e^2(t).dt = \int_0^t (\omega^*(t)-\omega(t))^2.dt \qquad 3.56$$

Where, ω^* is the reference speed.

ω is the real speed of the synchronous motor.

In this case, the block of the objective function is used to estimate the performances of the PI controller by minimizing this function.

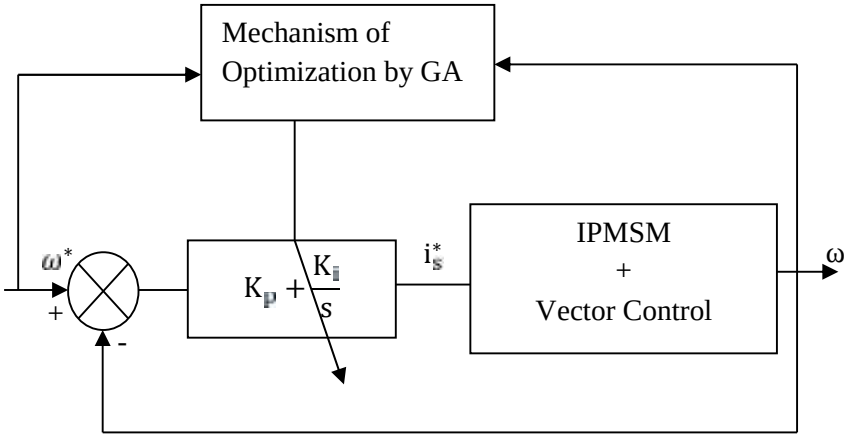

Figure 3.13. Structure of the technique of optimization of the PI controller by GA

The genetic algorithm parameters chosen for the tuning purpose are shown below.

Table 3.2
Parameters of GA

GA property	Value
Population size	60
Maximum number of generations	100
Crossover probability	0.8
Mutation probability	0.1
Tolerance	10^{-6}

After giving the above parameters to GA, the PI controller can be easily tuned and thus system performance can be improved. The parameters of the PI speed controller obtained according to the procedure of optimization by the technique of the GA are given below in Table 3.3

Table 3.3
PI controller gain values

Gain	K_p	K_i
Values	10.0	0.04

In this project, GA is used the value of K_p is fixed but K_i is variable.

By applying GA, at t= 0.23sec, the motor reaches to the command speed which shown in the Fig. 3.14(a). On the other hand, Fig. 3.14(b) shows that developed electromagnetic torque of the drive under starting condition. It is observed that higher electromagnetic torque is generated during the motor acceleration. Some oscillations in electromagnetic torque is noticed which is due to switching of the devices.

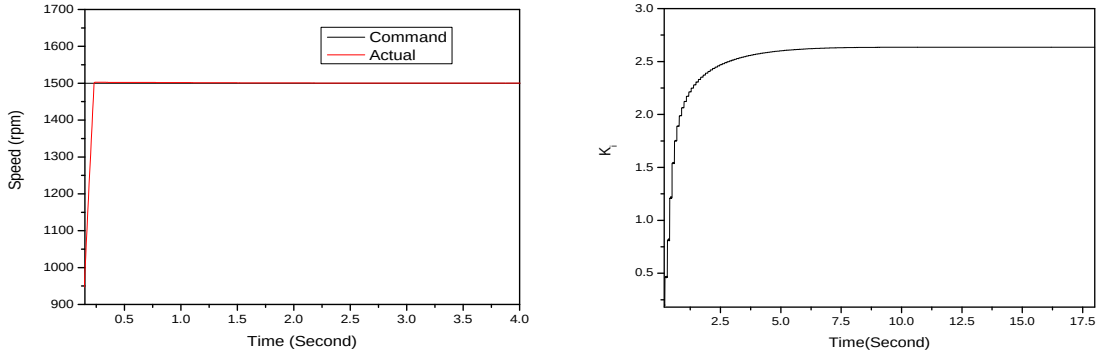

(a) (b)

Fig. 3.14 (a) Speed response of GA based PI controller and (b) The gain of K_i using GA

The difference between the speed response curves of natural algorithm vs. genetic algorithm, GA is faster than natural algorithm. About a half time of natural algorithm, the GA's speed response curve reaches to the command speed.

3.13 Advantages of using GA based PI

The advantages of using GA based PI is a novel probability optimization algorithm based on the concept. GA has a better characteristic of diversity in the population and can keep the balance of exploitation more easily- even with a small population. So GA has become a research hotpot in recent years.GA approach involves a population of individuals represented by strings of characters or digits.

3.14 Conclusion

In this chapter, mathematical models of IPMSM machines are established in both stationary reference frame and the rotating reference frame with respect to the IPMSM motors with and without saliency, e.g., IPM and SPM. By using the Park's Transformation, all time- varying inductances in the voltage equations are eliminated and in turn the models are simplified and vector control algorithms can be implemented. Using the 4S3P inverter model, the equations of the supplied voltage to the motor is obtained. Besides, control techniques of PI controller and hysteresis current controller are discussed clearly.

CHAPTER IV

Artificial Neural Network and Proposed Control System

4.1 Introduction

High performance drive systems using synchronous motors drives require the instantaneous knowledge of the positions of rotating phase variables. For field orientation, rotor flux magnitude and position information are very important to implement the control laws. There are several methods reported in the literature to estimate the rotor flux magnitude and position accurately and robustly. In this study Artificial Neural Network (ANN) based rotor flux estimator is proposed. A brief description of ANN's and their learning methods are described at the beginning of this chapter.

An ANN is an information processing paradigm that is inspired by the way biological nervous systems works, such as the brain process information. The key element of this paradigm is the novel structure of the information processing system. It is composed of a large number of highly interconnected processing elements (neurons) working in unison to solve specific problems. ANNs, like human beings, learn by example. An ANN is configured for a specific application, such as pattern recognition or data classification, through a learning process. Learning in biological systems involves adjustments to the synaptic connections that exist between the neurons. This is true for ANNs as well. The use of neural networks offers the following useful properties and capabilities:

- Nonlinearity
- Input-output mapping
- Adaptability
- Evidential response
- Contextual information
- Fault tolerance
- VLSI implementation
- Uniformity in analysis and design
- Neurobiological analogy

4.2 Models of a Neuron

A neuron is an information-processing unit that is fundamental to the operation of a neural network. The block diagram of Figure 4.1 shows the model of a neuron, which forms the basis for designing (artificial) neural networks. Here we identify three basic elements of the neuronal model:

- A set of **synapses or connecting links**, each of which is characterized by a weight or strength of its own. Specifically, a signal x_j at the input of synapse j connected to neuron k is multiplied by the synaptic weight $w_{kj.}$ It is important to make a note of the manner in which the subscripts of the synaptic weight w_{kj} are written. The first

subscript refers to the neuron in question and the second subscript refers to the input end of the synapse to which the weight refers. Unlike a synapse in the brain, the synaptic weight of an artificial neuron may lie in a range that includes negative as well as positive values.

- An adder for summing the input signals, weighted by the respective synapses of the neuron; the operations described here constitutes a linear combiner.

- An activation function for limiting the amplitude of the output of a neuron. The activation function is also referred to as a squashing function in that it squashes (limits) the permissible amplitude range of the output signal to some finite value.

The neuronal model of Fig. 4.1 also includes an externally applied bias, denoted by b_k. that has the effect of increasing or lowering the net input of the activation function, depending on whether it is positive or negative, respectively.

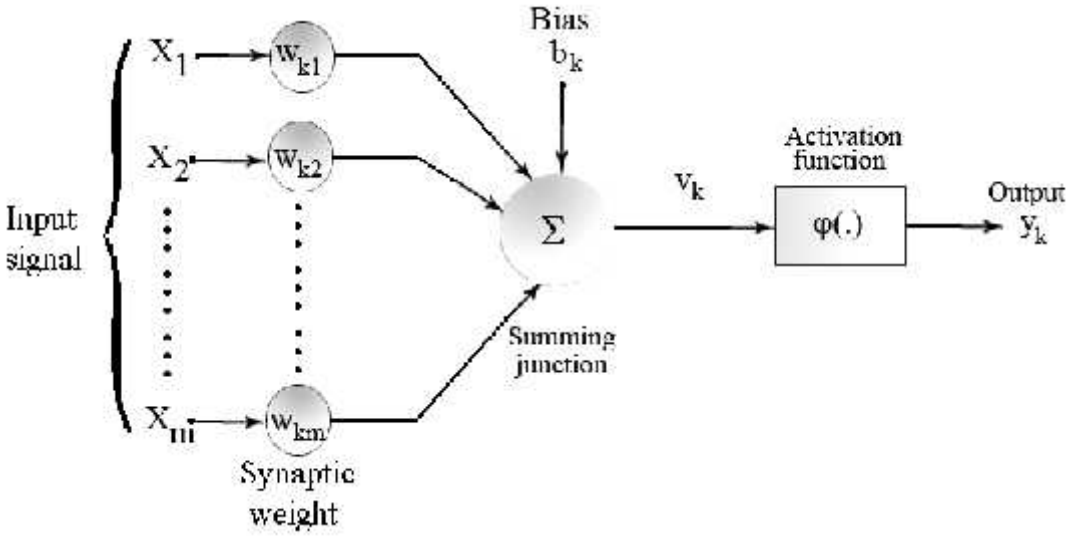

Figure 4.1 Nonlinear model of a neuron

In mathematical terms; a neuron *k* is written by the following pair of equations:

$$u_k = \sum_{j=1}^{m} w_k x_j \quad (4.1)$$

and

$$y_k = \varphi(u_k + b_k) \quad (4.2)$$

Where, $x_1, x_2, \ldots \ldots \ldots x_m$ are the input signals, $w_{k1}, w_{k2}, \ldots \ldots \ldots w_{km}$ are the synaptic weights of neuron k, u_k is the linear combiner output due to the input signals, b_k is the bias, $\varphi(.)$ is the activation function and y_k the output signal of the neuron.

The use of bias b_k has the effect of applying an affine transformation to the output u_k of the linear combiner in the model of Figure 3.1, as shown by:

$$v_k = u_k + b_k \tag{4.3}$$

In particular, depending on whether the bias b_k is positive or negative, the relationship between the induced local field or activation potential v_k of neuron k and the linear combiner output u_k *is* modified in the manner will be illustrated later*;* hereafter the term "induced local field" is used . It can be noted that as a result of this affine transformation, the graph of v_k versus u_k no longer passes through the origin.

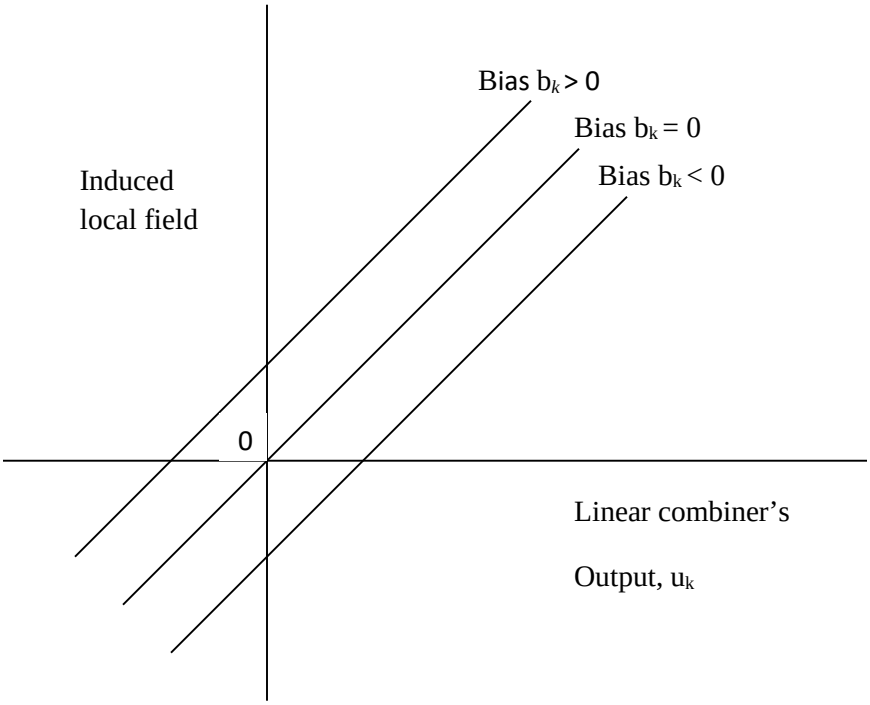

Figure 4.2 Affine transformations produced by the presence of a bias;

Where $v_k = b_k$ at $u_k = 0$

The bias b_k is an external parameter of artificial neuron k. We may account for its presence as in (4.2). Equivalently, we may formulate the combination of (4.1) to (4.3) as follows:

$$v_k = \sum_{j=1}^{m} w_k x_j \tag{4.4}$$

And

$$y_k = \varphi(v_k) \tag{4.5}$$

In Eq. (3.4) we have added a new synapse. Its input is:

$$X_0 = +1 \tag{4.6}$$

and its weight is:

$w_{k0}=b$ (4.7)

We may therefore, reformulate the model of neuron k as in Fig. 3.3. In this figure, the effect of the bias is accounted for by doing any two view points:

(1) Adding a new input signal fixed at +1, and
(2) Adding a new synaptic weight equal to the bias b_k.

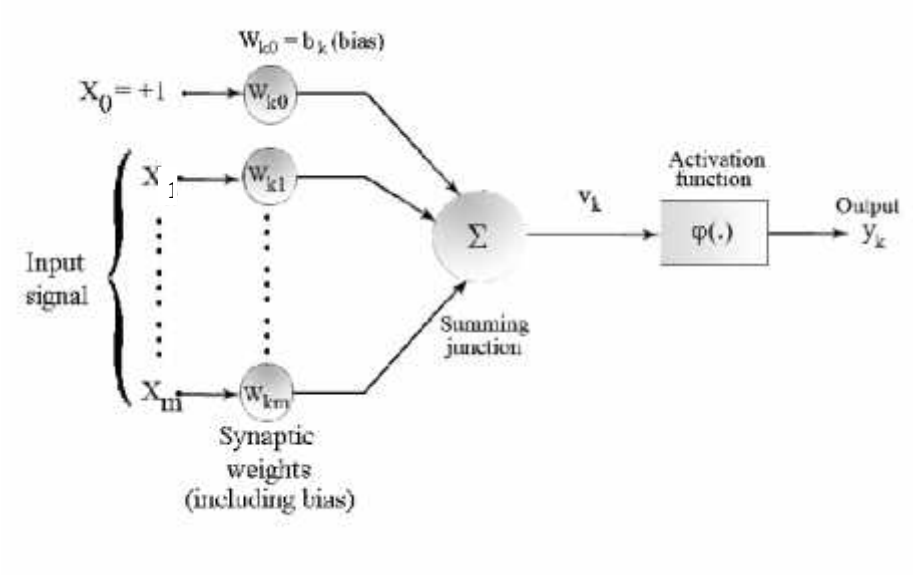

Figure 4.3 Another nonlinear model of a neuron

Although the models of Figs. 4.1 and 4.3 are different in appearance, they are mathematically equivalent.

4.3 Learning in Neural Networks

The property that is of primary significance for a neural network is the ability of the network to learn from its environment, and to improve its performance through learning. A neural network learns from its environment through an interactive process of adjustments applied to its synaptic weights and bias levels. Ideally, the network becomes more knowledgeable about its environment after every iteration of learning process.

The definition of learning in the context of neural network is:

Learning is a process by which the free parameters of a neural network are adapted through a process of simulation by the environment in which the network is embedded. The type of learning is determined by the manner in which the change of parameters takes place.

4.4 Real Time Recurrent Learning Algorithm

The property that is of primary significance for a neural network is the ability of the network to learn from environment, and to improve its performance through learning. A neural network learns from its environment though an interactive process of adjustments applied to its synaptic weights and bias levels. Ideally, the network becomes more knowledgeable about its environment after every iteration of learning process. The definition of learning in the context of neural network is [35]: "Learning is a process by which the free parameters of a neural network are adapted through a process of simulation by the environment in which the network is embedded. The type of learning is determined by the manner in which the change of parameters takes place."

The RTRL algorithm derives its name from the fact that adjustments are made to the synaptic weights of a fully connected recurrent network in real time. Fig. 4.4 shows the layout of such a recurrent network [35].

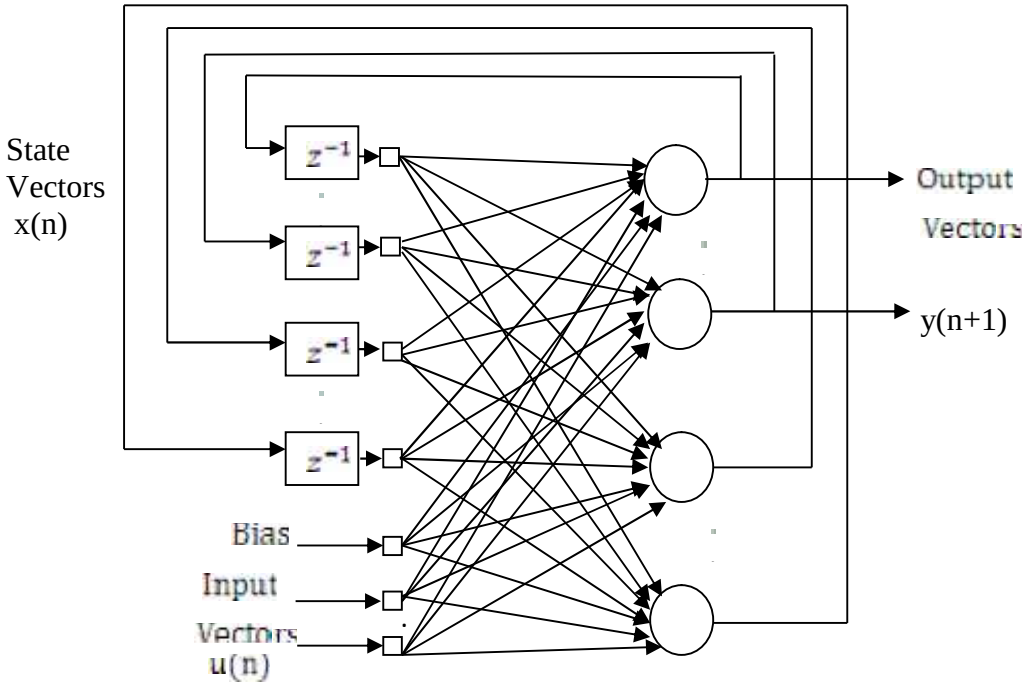

Figure 4.4 Fully connected real time recurrent network

4.4.1 Real Time Recurrent Neural Network (RTRNN)

A recurrent neural network (RNN) is a class of neural network where connections between units form a directed cycle. This creates an internal state of the network which allows it to exhibit dynamic temporal behavior. RNNs can use their internal memory to process arbitrary sequences

of inputs. This makes them applicable to tasks such as unsegmented connected handwriting recognition.

The flux components are estimated stationary α-,β-axis stator currents and speed error, E_ω. An equivalent RTRNN is proposed which results in the following matrix equation [36]:

$$\begin{bmatrix}\lambda_{\alpha s}(k+1)\\ \lambda_{\beta s}(k+1)\end{bmatrix} = \begin{bmatrix}W_1 & 0\\ 0 & W_2\end{bmatrix}\begin{bmatrix}\lambda_{\alpha s}(k)\\ \lambda_{\beta s}(k)\end{bmatrix} + \begin{bmatrix}W_1\\ W_2\end{bmatrix} i_{\alpha s}(k) + \begin{bmatrix}W_1\\ W_2\end{bmatrix} i_{\beta s}(k) + \begin{bmatrix}W_1\\ W_2\end{bmatrix} E_\omega(k) \qquad 4.8$$

Where W_1 , W_2 , W_1 , W_2 etc. is the weight of the RTRNN, which is shown in Fig. 4.3.

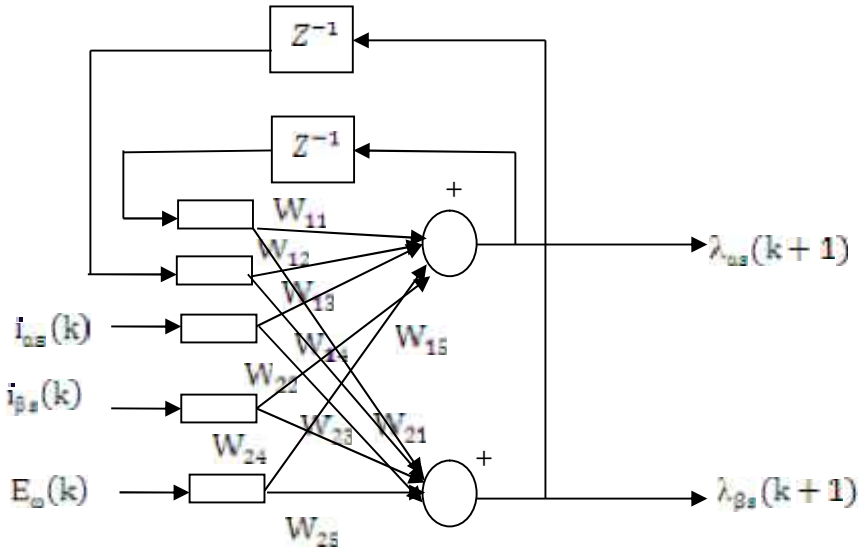

Figure 4.5 Stationary α- and β- axis stator flux estimation by Real Time Recurrent Neural Network (RTRNN)

The RNN weights are dependent on the sampling frequency of the control system: this means that a retraining of the RNN is required if the sampling frequency varies.

4.5 Proposed IPMSM Control Scheme

Simulation of the drive system is carried out in C++ environment. For the simulation, the project used a IPMSM model equation, in this model, used control input voltage to run the machine. The difference between command speed and the actual speed creates the speed error

The motor speed error is processed through a **PI** controller to generate the torque producing component of the stator current ($\mathbf{i_q^*}$)**.** The PI controller is tuned using **GA** to get further fast speed response of synchronous motor. The magnetizing component of the stator currents $\mathbf{i_d^*}$ is obtained from the flux program. $\mathbf{i_d^*}$ and $\mathbf{i_q^*}$ are then used to generate the reference current $\mathbf{i_\alpha^*}$ and $\mathbf{i_\beta^*}$.

The rotor angle requires for vector rotation is obtained from RTRNN based flux and angle estimate. Two independent hysteresis current controllers with a suitable hysteresis band are used to command the motor current $\mathbf{i}_{\alpha}^{*}$ and $\mathbf{i}_{\beta}^{*}$ to follow the reference currents. The hysteresis controllers also generate four switching signals which fire the power semiconductor devices of the three phase inverter to produce the actual voltages to the motor.

The three phase motor currents $\mathbf{i}_a$, $\mathbf{i}_b$ and $\mathbf{i}_c$ are transformed into **α-** and **β**-axis components through Clarke's transformation. A speed transducer is used to measure the speed of the IPMSM accurately.

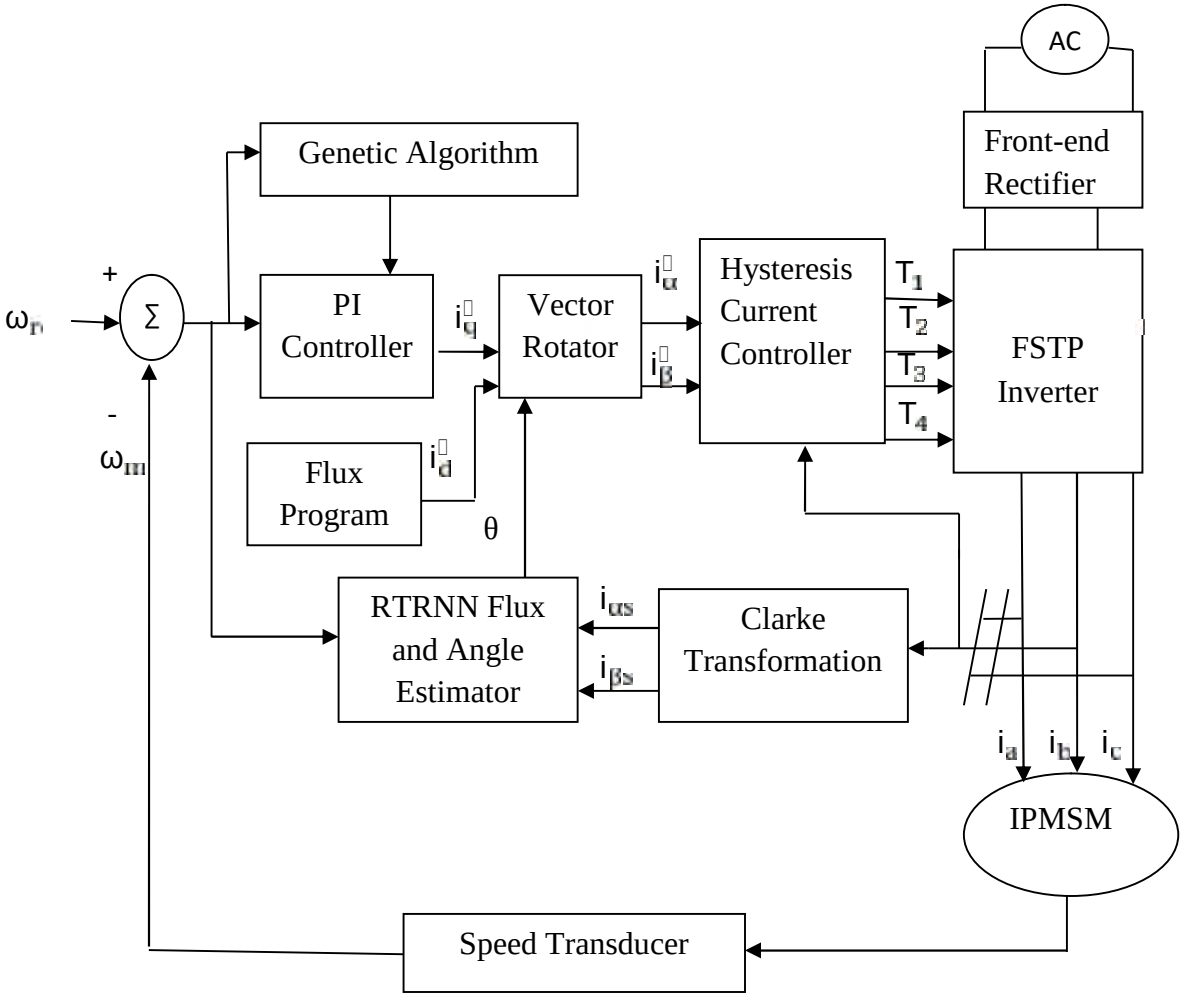

Fig.4.6 Proposed control scheme of the IPMSM

4.5.1 Adjusting the PI Gains

When tuning a PI controller for first time, the I gain is set to zero. Then the P gain is increased until the system responses well to set point changes without excessive overshoot. Using lower values of P gain will" loosely" control the system, while higher values will give 'tighter' control. At this point, the system will probably not converge to the set point. After selecting a reasonable

value of P gain, the I gain is increased slowly to force the system error to zero. Only a small amount of I gain is required in most systems.

The effect of I gain, if large enough, can overcome the action of the P term, slow the overall control response and cause the system to oscillate around the set point. If oscillation occurs, reducing the I gain and increasing the P gain will usually solve the problem. There is a single PI control loop in this application. The selection of suitable values for gain constants is carried out for different combinations of K_p and K_I after having their initial guesses following the ideas in [37]

4.5.2 Flux Program

In constant- torque region the torque can be controlled by i_t whereas stator flus (λ_s) can be maintained at a value determined by the flux program. The proposed control system incorporates a flux control loop where the stator flux command (λ_s^*) is generated through the flux program. The flux loop then generates magnetizing component of the stator current (i_m^*) and helps maintaining the desired λ_s irrespective of variation effect.

4.5.3 Coordinate Transforms

4.5.3.1 Vector Rotator

The first coordinate transform, called the vector rotator, moves a two axis, two dimensional coordinate system, referenced to the stator, onto a three axis system, keeping the same reference. In this application, the command i_m^* and i_t^* signals are processes through vector rotator to generate the three phase current commands for the hysteresis current controller. The stationary axes a-, b- c- their two phase equivalents α-,β- and the rotating axes of the IPMSM are shown in Fig. 4.5.

The reference currents are formulated as follows:

$$i_a^* = i_m^* \cos\theta - i_t^* \sin\theta \quad (4.9)$$

$$i_b^* = i_m^* \cos(\theta - 120^o) - i_t^* \sin(\theta - 120^o) \quad (4.10)$$

$$i_c^* = i_m^* \cos(\theta + 120^o) - i_t^* \sin(\theta + 120^o) \quad (4.11)$$

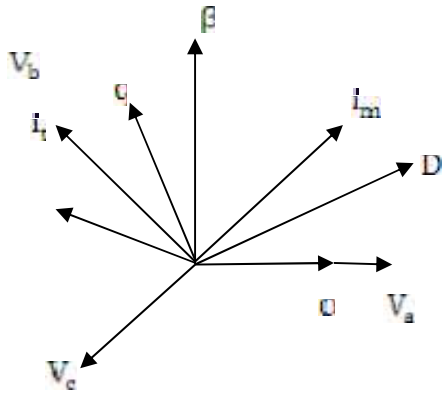

Figure 4.7 Stationary and rotating axes of IPMSM

4.5.3.2 Clarke Transform

The Clarke transform converts the stationary 3- axes (a-,b-,c-) quantities by the following equations:

$$i_{\alpha s} = i_a - \frac{1}{2} i_b - \frac{1}{2} i_c \quad (4.12)$$

$$i_{\beta s} = \frac{\sqrt{3}}{2} (i_b - i_c) \quad (4.13)$$

4.5.4 Hysteresis current controller Techniques

A typical three-phase hysteresis current controller is shown in Fig.4.8 with -switch SW turned off. The hysteresis controller is used to control the current in such a way that it can follow the command current with a hysteresis band. In the case of the hysteresis controller, the switching frequency varies over the fundamental period. Because of this varying switching frequency, the inverter operation is irregular and hence the switching losses also increase. This problem arises

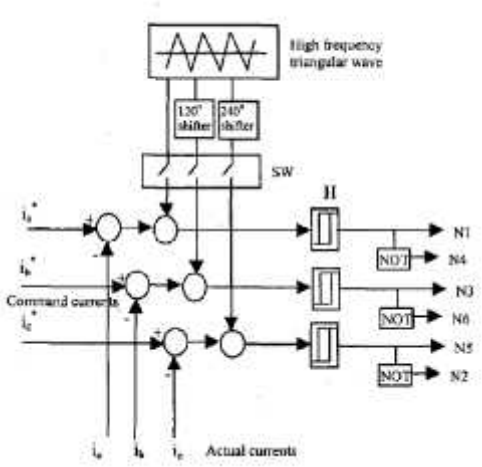

Fig.4.8 General current controller scheme.

specially at a low speed condition where the back emf is low. This results in higher harmonic currents at the low speed condition, which may result in instability. Based on the hysteresis band conventionally there are two types of hysteresis controllers, namely, fixed band and sinusoidal band hysteresis controllers. In the sinusoidal band, the hysteresis band varies sinusoidally over the fundamental period. The advantage of this scheme is that the harmonic content of the current decreases. The disadvantage is that the switching frequency near zero crossing is very high [38]. As a result, the maximum switching frequency of the inverter increases. In the case of the fixed band controller, the maximum switching frequency of the inverter is reduced but the harmonic current is increased. In order to compromise between the maximum inverter switching frequency and harmonic content of the current, the mixed band hysteresis controller is used. In the mixed band controller, the hysteresis band varies sinusoidally around the reference and a constant value as shown. Consider that N1, N3 and N5 are the logic signals for the high transistors of the inverter and N4, N6 and N2 are the logic signals for the low transistors of the inverter, respectively. When the logic signal N1 is 1 then the transistor TI is on and when it is 0 then TI is

off. Similar logic is valid for other five logic signals. The control logic of hysteresis controller can be described as follows:

1. For $i_a^*>0$: $N_4=0$, if $i_a > i_u$, then $N_1=0$, else if $i_a > i_l$, then $N_1=1$
2. For $i_a^*<0$: $N_1=0$, if $i_a > i_u$, then $N_4=1$, else if $i_a < i_l$, then $N_4=0$

Where, i_a is actual 'a' phase current, i_a^* is command current, $i_u = i_a^*+H$, is upper band, $i_l = i_a^*-H$, is lower band and H is the hysteresis band. For a fixed band $H=\alpha$, for a sinusoidal band $H=\alpha^*\sin(\omega t)$, and for a mixed band $H=\beta+\alpha^*\sin(\omega t)$, where α and β are constant.

4.5.4.1 Ramp Comparator Controller

A typical three-phase conventional ramp comparator controller is also shown in Fig.4.10 with switch **SW** 'on' and bypassing the phase shifter. In the ramp comparator controller, the error signals between the actual motor currents and the respective command currents are compared to a high frequency triangular waveform of fixed frequency and amplitude. The control logic for the ramp comparator controller can be described as follows:

1. For $i_a^*>0$: $N_4=0$, if $e_a > (i_t + band)$, then $N_1=1$, else $N_1=0$
2. For $i_a^*<0$: $N_1=0$, if $e_a > (i_t - band)$, then $N_4=1$, else $N_4=0$

Where, $e_a = i_a^* - i_a$ is the 'a' phase current error and i_t, is the high frequency triangular wave. In order to prevent the multiple crossings of error signals with triangular waveform some hysteresis band has been added to the controller. Because of the fixed frequency of the triangular wave, the switching frequency of the inverter remains fixed. This is the advantage of this controller. However, the disadvantages of this controller are that the actual motor current has some amplitude and phase errors, which become acute at the high speed condition. Moreover, sometimes the motor is disconnected from the supply over the fundamental period when a zero voltage vector is applied to the motor.

4.5.4.2 Improved Ramp Comparator Controller

In order to overcome the previously mentioned difficulties of the conventional ramp controller, an improved ramp comparator controller is used. The schematic diagram of this controller is shown in Fig.3. In this controller, the current error signals are compared to three 120° phase shifted triangular waveforms having the same fixed frequency and amplitude. The performance is identical to three independent single-phase ramp comparator controllers. **As** there is no interaction between the three phases, it removes the zero voltage vectors for balanced operation.

4.6 Conclusion

In this chapter an idea concerning position sensorless control has been presented. The aim of this research was top find a position estimation scheme for the IPMSM that is capable of working under all operating conditions, i.e. from zero to high speed and zero to full load. Therefore, a RNN based stator flux and rotor position estimator is proposed. Beside this, the application of PI controller and hysteresis current controller in the vector control of the IPMSM drive is described briefly.

CHAPTER V

Simulations Results and Discussions

5.1 Introduction

This chapter deals with the simulation results of the IPMSM drive system. A simulation study is conducted in order to test the performance of the drive system. The system under consideration is simulated in C++ environment. The machine model is considered in d-q axes frame. The state space equations are solves with Runge- Kutta-Gill subroutine. The sampling time for simulating the system is 5μs. Reference phase currents are generated from the torque and magnetizing currents i_t^* and i_m^*. The phase voltages V_a, V_b and V_c resulting from the hysteresis currents controller are transformed into d- and q- axis quantities V_d and V_q. Currents obtained from simulation model are transferred to get the actual phase currents. The rating and motor parameters used in this simulation are given in Appendix. The simulation results for different operating conditions are listed in the subsequent sections.

5.2 RNN based Stator Flux and Rotor Position Estimation

Simulation studies for proposed high performance synchronous motor control are presented in this chapter. The gain coefficients of PI controller are optimized using proposed GA algorithm. "Learning is a process by which the free parameters of a neural network are adapted through a process of simulation by the environment in which the network is embedded. The type of learning is determined by the manner in which the change of parameters takes place." The effectiveness of the proposed flux estimator along α-β axes needs to be verified before implementing it in the drive system. The weights of the RNN are obtained by training the neural network by CRTRL algorithm and are provided in Appendix. Real time flux components calculated from exact values of motor variables are computed and compared with the estimated flux components. Figs. 5.1.1 and 5.1.2 give a component between the actual and estimated values of α-β axes stator fluxes and rotor angle for the 4S3P inverter fed drive under transient and steady- state conditions when the motor runs at 1500 rpm. Fig. 5.1.3 gives a component between the actual and estimated values of the stator fluxes and rotor angle for the 4S3P inverter fed drive when the motor runs at 1500 rpm. A complete matching of the variables is indicated in the figures.

Clearly, the proposed RNN estimator can be used to accurately estimate stator flux components and rotor angle at both high- and low- speeds. Improvements of the performance of the drive systems are given at the finishing part of the chapter

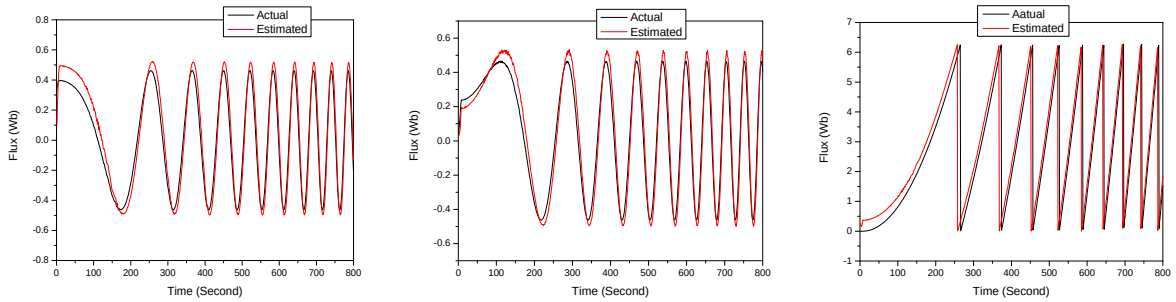

(a) (b) (c)

Figure 5.1.1 Actual and Estimated responses of (a) α-axis stator flux, (b) β- axis stator flux, and (c) Rotor angle for the 4S3P inverter fed IPMSM drive (runs at 1500 rpm) under transient condition.

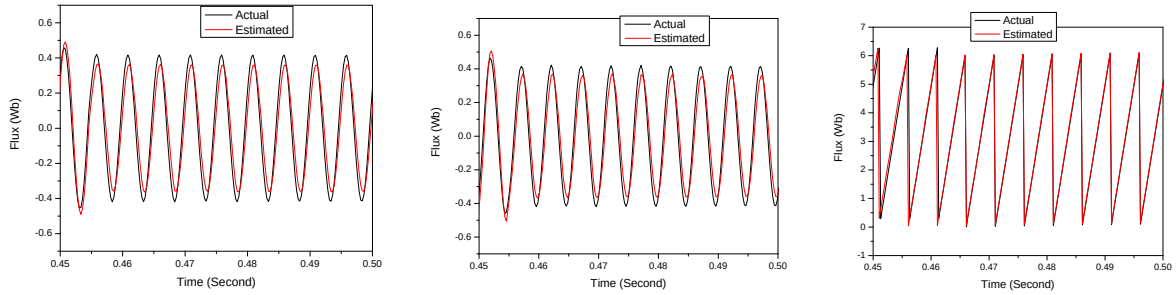

(a) (b) (c)

Figure 5.1.2 Actual and Estimated responses of (a) α-axis stator flux, (b) β- axis stator flux, and (c) Rotor angle for the 4S3P inverter fed IPMSM drive (runs at 1500 rpm) under steady –state condition.

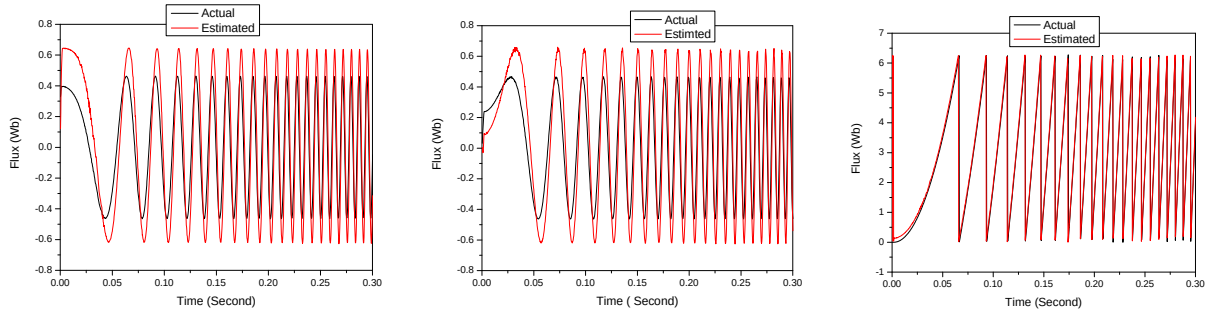

(a) (b) (c)

Figure 5.1.3 Actual and Estimated responses of (a) α-axis stator flux, (b) β- axis stator flux, and (c) Rotor angle for the 4S3P inverter fed IPMSM drive (runs at 1500 rpm) under transient and steady –state conditions.

5.3 Starting Performance of the IPMSM Drive

The motor was started with a command speed of 1500 rpm and load torque of 1.0 N.m from standstill condition. Fig. 5.2 show the stator voltages supplied to the motor by the 4S3P inverter. In case of 4S3P inverter the a-phase and b-phase voltages have almost similar characteristics but the c-phase voltage is different in nature. Therefore, the 3- phase voltages produced by the 4S3P inverter are in unbalanced condition.

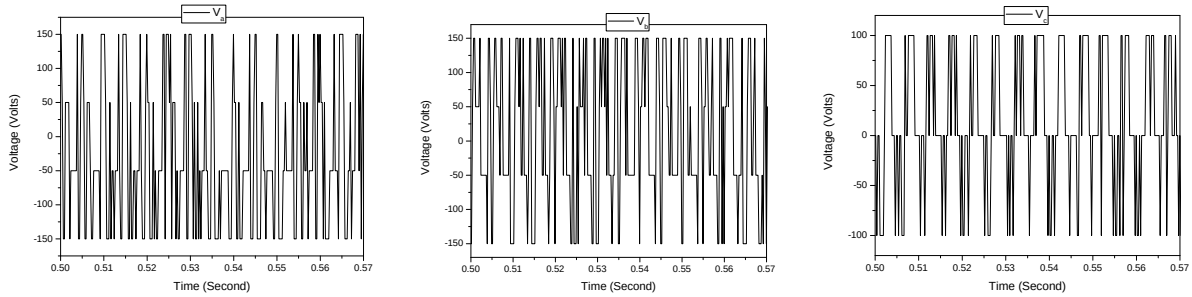

(a) (b) (c)

Figure 5.2 Stator phase voltages for the 4S3P inverter fed IPMSM: (a) $V_{a,}$, (b) $V_{b,}$ (c) V_c

Fig. 5.3 show the speed response, developed electromagnetic torque, command currents and actual motor currents for the IPMSM drive with 4S3P inverter. In case of the actual speed follows the command speed accurately without steady- state error and oscillations. It is observed that higher electromagnetic torque is developed during the motor acceleration. Some oscillations in electromagnetic torque is noticed which is due to switching of the devices with hysteresis controller. Difference between developed and load torques is due to viscous damping torque of the drive system. The three phase command currents are obtained vector rotator. The three phase actual motors currents are obtained using Park's transformation. It is noticed that the motor follows the command currents efficiently. The currents obtained from 4S3P inverter fed drive seem to be slightly non- sinusoidal in nature. But this unbalanced characteristic of the 4S3P inverter does not hamper the speed response of the drive.

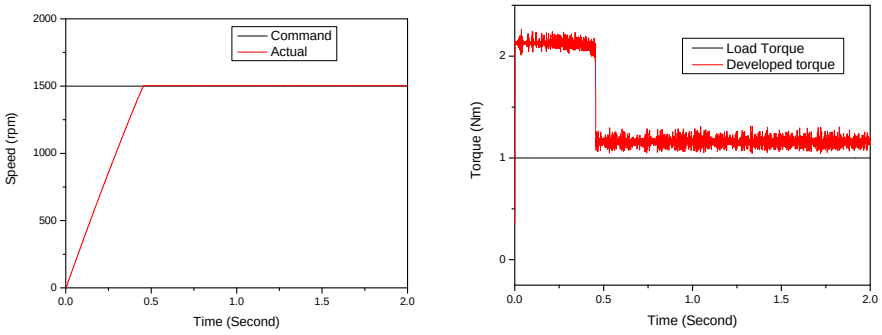

(a) (b)

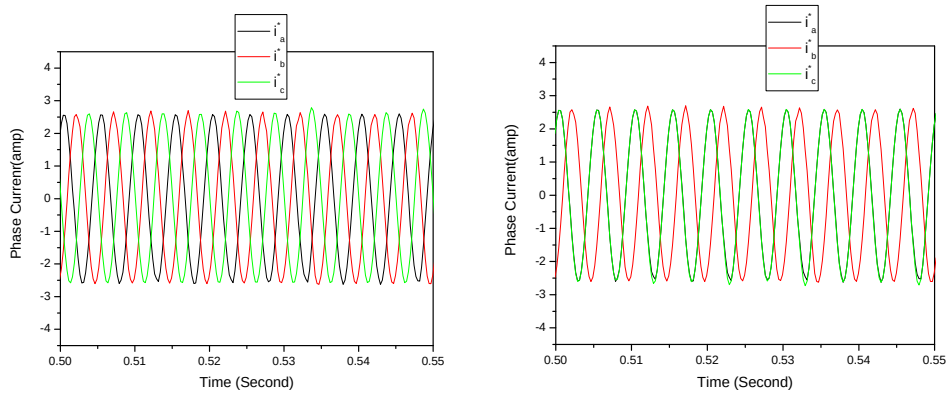

(c) (d)

Figure 5.3 (a) Speed, (b) Developed electromagnetic torque, (c) Command currents, and (d) actual motor currents for the 4S3P inverter fed IPMSM drive.

5.4 Performance under Different Operating Conditions

The performance of the IPMSM drive under different operating conditions with GA and compare the performance of speed response curve was also investigated in order to verify the robustness of the proposed control scheme. The corresponding responses and their descriptions are given in the following sub- sections.

5.4.1 Sudden Change of Load Torque

Initially the motor was started from standstill with load torque 1 N.m. The estimated rotor angle and the speed responses for change of load torque are given in Figs. 5.4(a) and (b).The speed response curve reached to the command speed at t=0.45sec. Sudden change of load torque does not affect the position estimation and causes a negligible oscillation in speed. Figs 5.4(c) and (d) show the corresponding torque and motor currents. The motor currents increase after 1.0 second due to the increase of load torque.

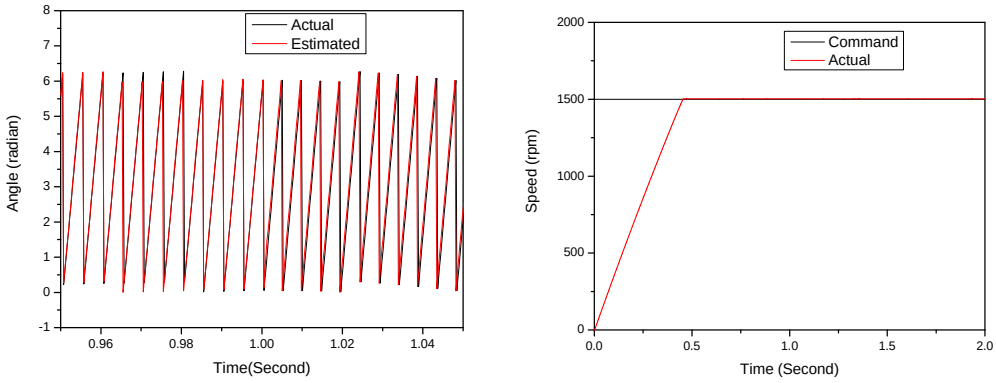

(a) (b)

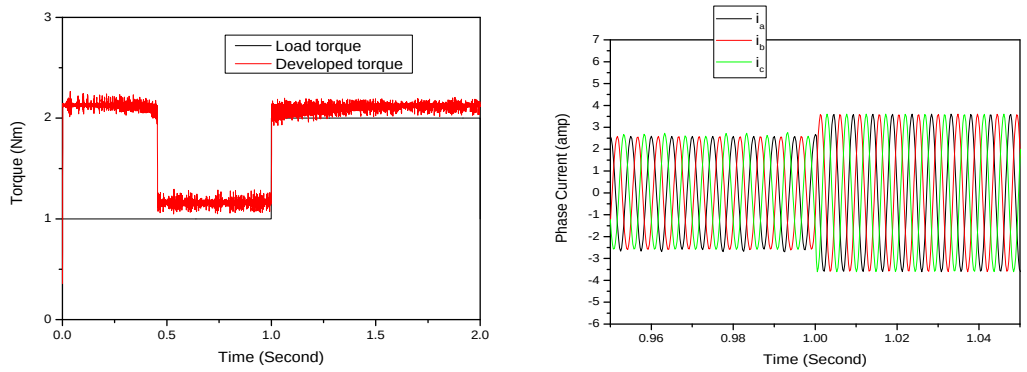

(c) (d)

Figure 5.4 (a) Estimated rotor angle, (b) Speed, (c) Developed electromagnetic torque, and (d) Three Phase currents for the proposed IPMSM drive for change of load torque.

By applying GA,

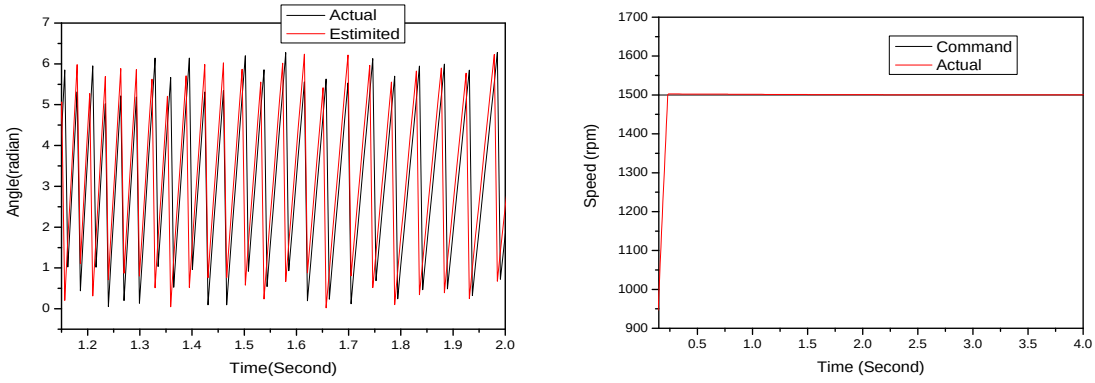

(a) (b)

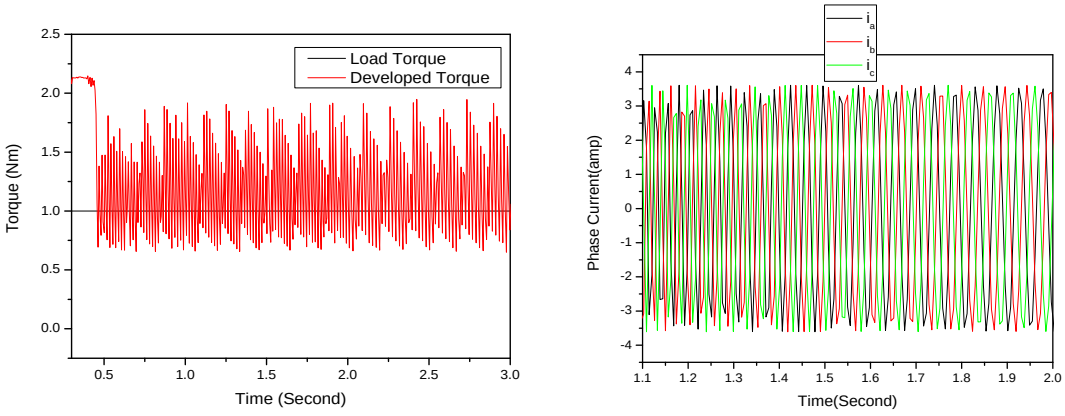

(c) (d)

Figure 5.5 (a) Estimated rotor angle, (b) Speed, (c) Developed electromagnetic torque, and (d) Three Phase currents for the proposed IPMSM drive for change of load torque by using GA.

By applying GA the motor was stared from standstill with load torque 1N.m. The estimated rotor angle and the speed responses for the change of load torque are given in Figs. 5.5(a) and (b). The speed response curve reached to the command speed at t=0.23sec. Sudden change of load torque does not affect the position estimation and causes a negligible oscillation in speed. Figs 5.5(c) and (d) show the corresponding torque and motor currents.

It is observed that GA based system needs t=0.23sec to speed up that motor at reference speed 1500 rpm, whereas Natural Algorithm based system needs t=0.45 sec.

5.4.2 Variation of Stator Parameters

To observe the effect of parameter variations, the motor stator resistance was doubled (keeping other parameters constant) at t=1.0 second. Fig. 5.6(a) shows the effect of stator resistance change on angle estimation. The estimated angle still follows the actual angle. Thus the change in resistance has negligible effect on the accuracy of rotor position estimation. Fig. 5.6(b) shows the effect of stator resistance change on speed response. The speed dose not drops at all due to change of stator resistance. The speed response curve reached to the command speed at t=0.45sec. Thus the drive performance is insensitive of stator parameter variation. Figs. 5.6(c) and (d) show that the developed torque and motor currents are also insensitive to stator parameter variation.

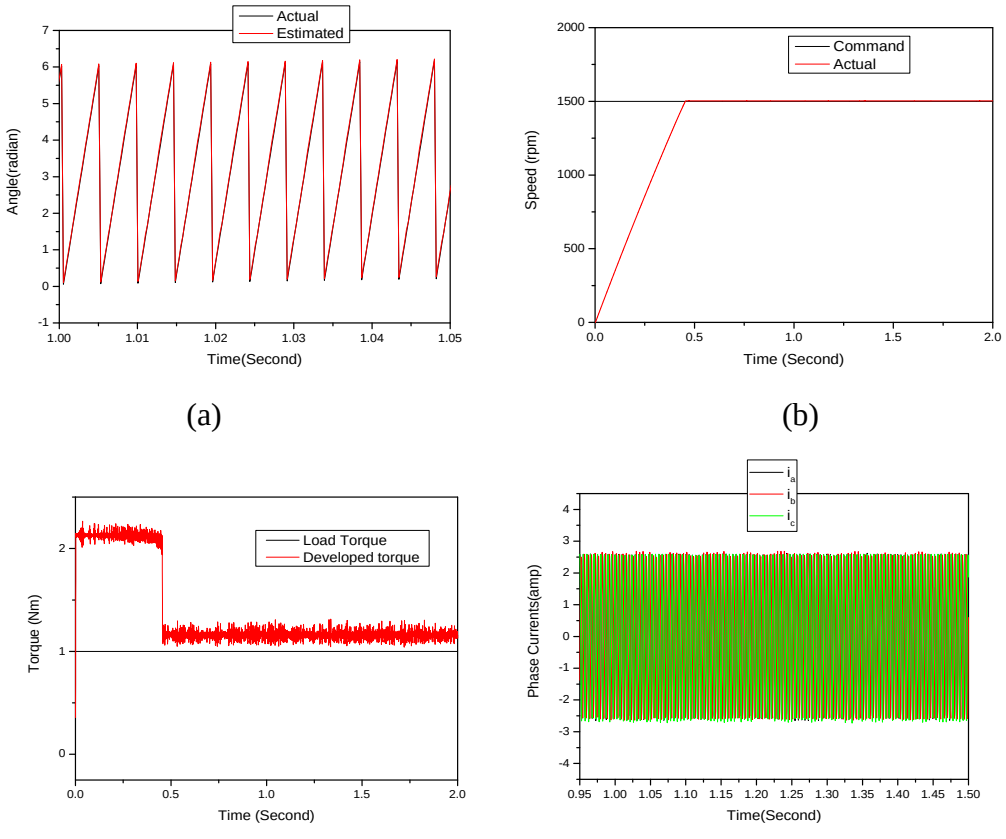

Figure 5.6 (a) Estimated rotor angle, (b) Speed, (c) Developed Electromagnetic torque, and (d) Three phase currents for the proposed IPMSM drive for change of stator resistance.

By applying GA,

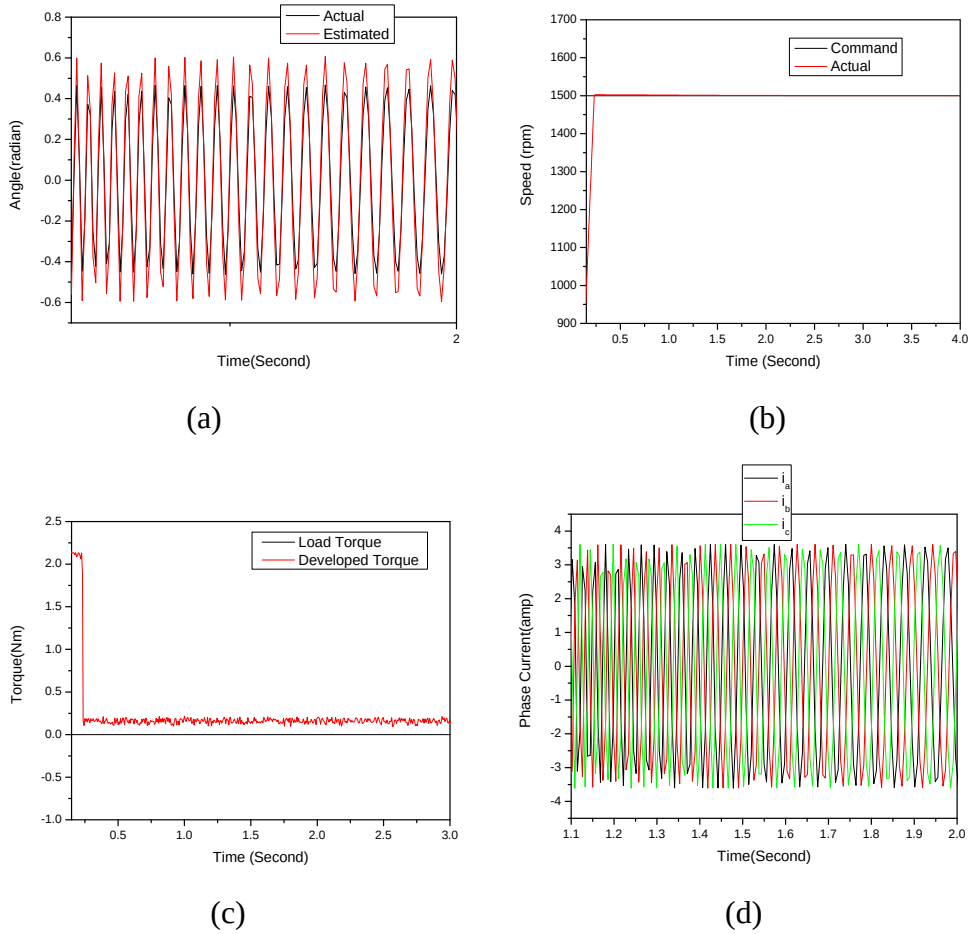

Figure 5.7 (a) Estimated rotor angle, (b) Speed, (c) Developed Electromagnetic torque, and (d) Three phase currents for the proposed IPMSM drive for change of stator resistance by using GA.

Fig. 5.7(a) shows the effect of stator resistance change on angle estimation. The change in resistance has negligible effect on the accuracy of rotor position estimation. Fig. 5.7(b) shows the effect of stator resistance change on speed response. The speed dose not drops at all due to change of stator resistance. The speed response curve reached to the command speed at t=0.23sec. Figs. 5.7(c) and (d) show that the developed torque and motor currents are also insensitive to stator parameter variation.

It is observed that GA based system needs t=0.23sec to speed up that motor at reference speed 1500 rpm, whereas Natural Algorithm based system needs t=0.45 sec.

5.4.3 Speed Reversal

Speed reversal is an essential requirement for high performance IPMSM drives. Therefore, to monitor the effect of speed reversal, the command speed of the motor was reversal from 1500 rpm to -1500 rpm at t=0.6 second and again to 1500 rpm at t=1.4 second. Fig. 5.8(a) shows

estimated rotor angle when the motor runs at -1500 rpm. There is slight error between the estimated and actual angle but it is within the acceptable limit. The speed response for different set speeds is shown in Fig.5.8 (b). The speed response curve reached to the command speed at t=0.45sec. It is observed that the drive system follows both the forward and reverse direction, reference track very quickly. The impact on developed electromagnetic torque and motor current due to speed reversal is shown in Fig. 5.8(c) and (d). The proposed control scheme produces less torque fluctuation at steady- state condition.

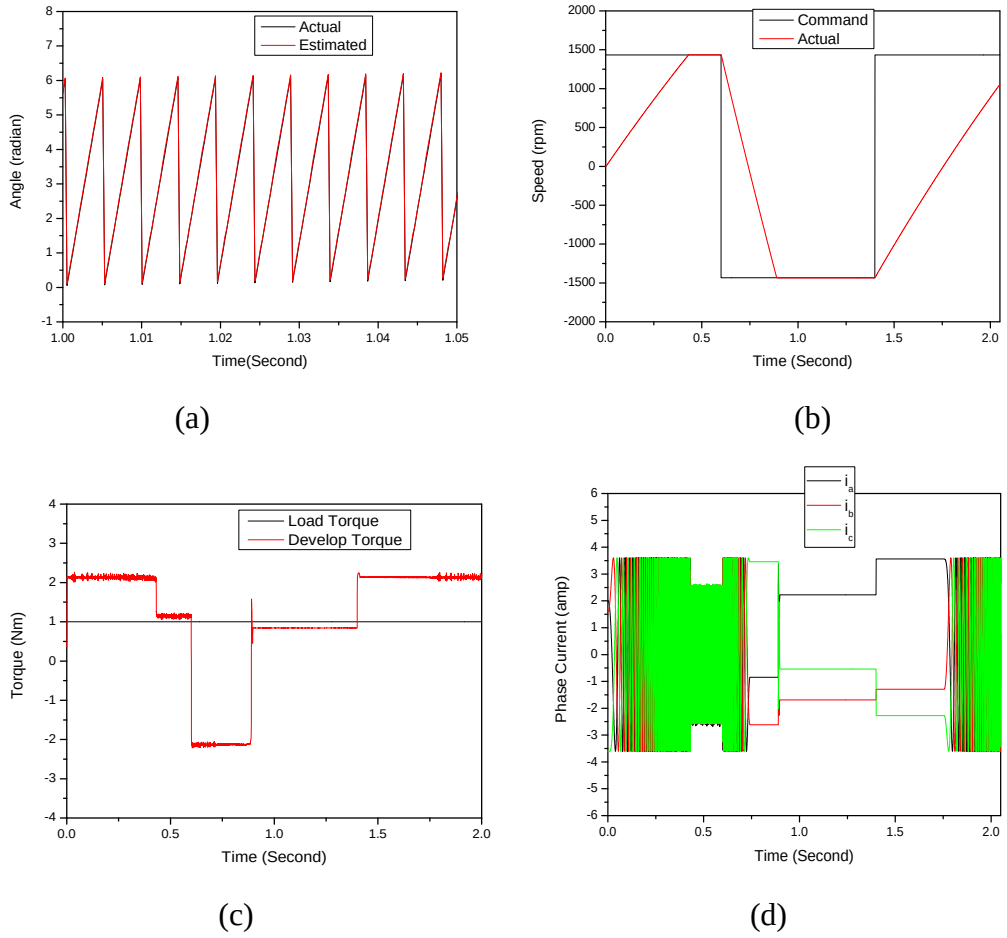

Figure 5.8 (a) Estimated rotor angle, (b) Speed, (c) Developed electromagnetic torque, and (d) Three phase currents for the proposed IPMSM drive under speed reversal.

By applying GA

Speed reversal is an essential requirement for high performance IPMSM drives. Fig. 5.9(a) shows estimated rotor angle. The speed response for different set speeds is shown in Fig.5.9 (b). The speed response curve reached to the command speed at t=0.22sec. It is observed that the drive system follows both the forward and reverse direction reference track very quickly. The impact on developed electromagnetic torque and motor current due to speed reversal is shown in

Fig. 5.9(c) and (d). The proposed control scheme produces less torque fluctuation at steady- state condition.

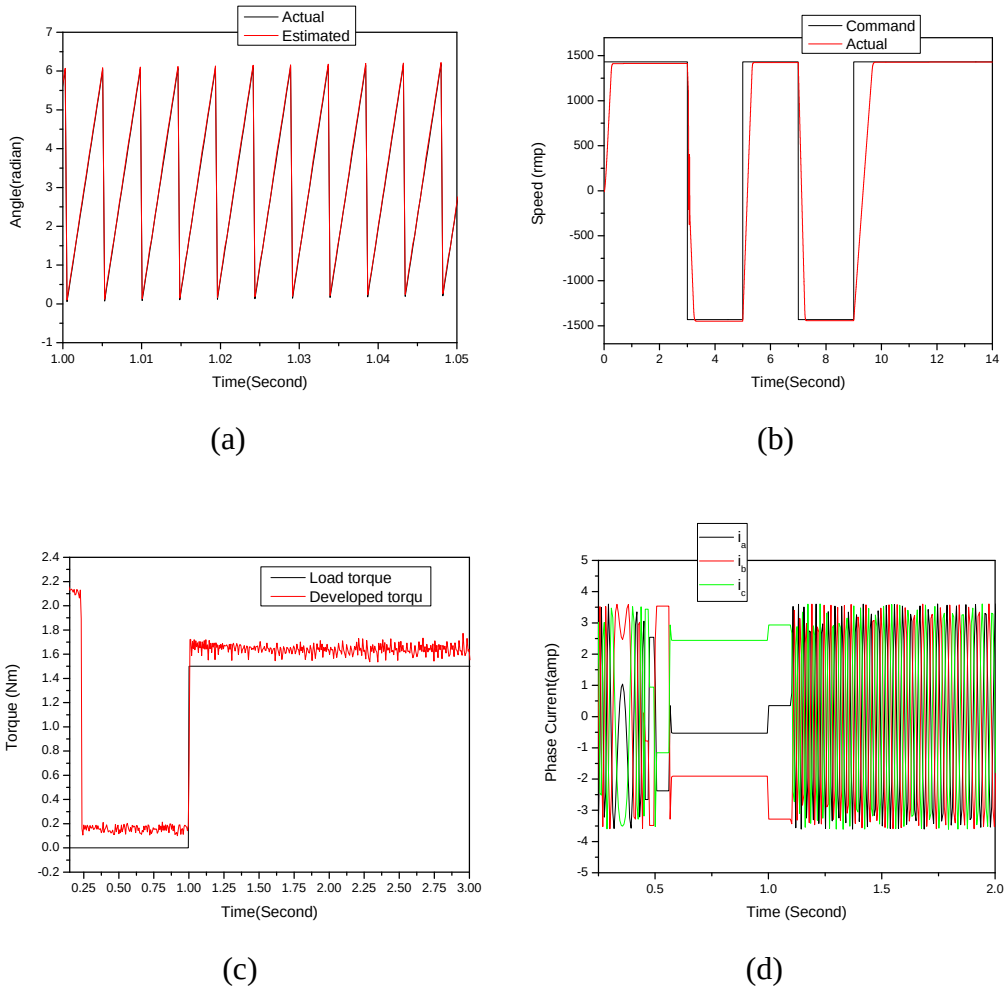

Figure 5.9 (a) Estimated rotor angle, (b) Speed, (c) Developed electromagnetic torque, and (d) Three phase currents for the proposed IPMSM drive under speed reversal by using GA.

It is observed that GA based system needs t=0.23sec to speed up that motor at reference speed 1500 rpm, whereas Natural Algorithm based system needs t=0.45 sec.

5.4.4 Ramp Speed Change

Like as speed reversal, ramp speed is also is an essential requirement for high performance IPMSM drives. The controller set speed was gradually increased from zero and at time t=1.0 second it remained constant to 1500 rpm value. The estimated rotor position, speed response, developed electromagnetic torque and motor currents are shown in Fig. 5.10. The motor follows the command speed from the starting without any oscillation and steady- state error. The developed torque response is also similar to the starting performance.

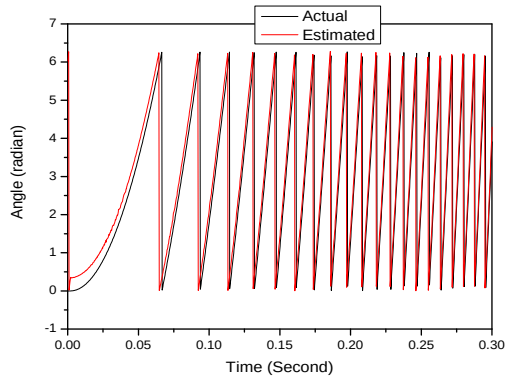

(a)

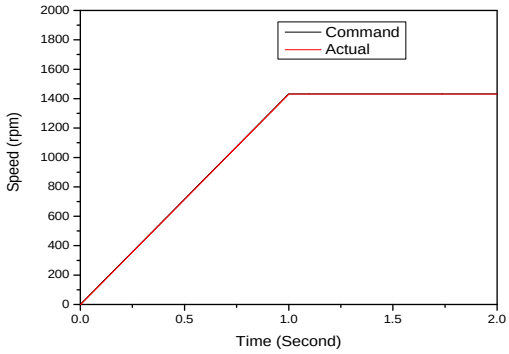

(b)

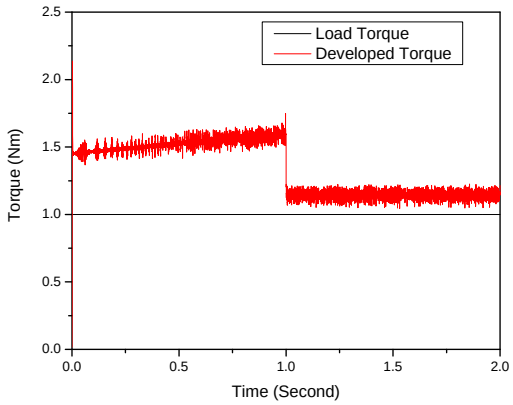

(c)

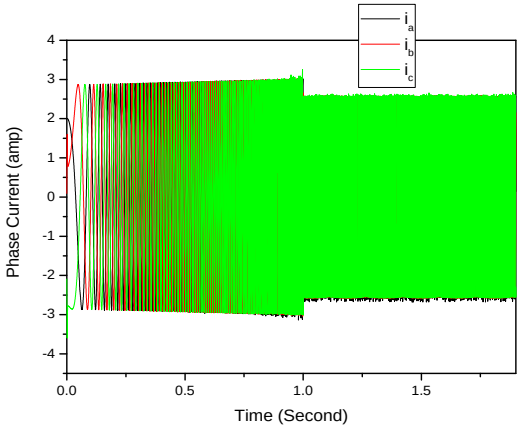

(d)

Figure 5.10 (a) Estimated rotor angle, (b) Speed, (c) Developed electromagnetic torque, and (d) Three phase currents for the proposed IPMSM drive under speed ramp speed change.

By using GA,

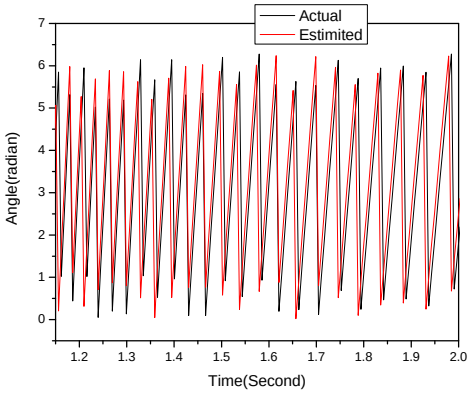

(a)

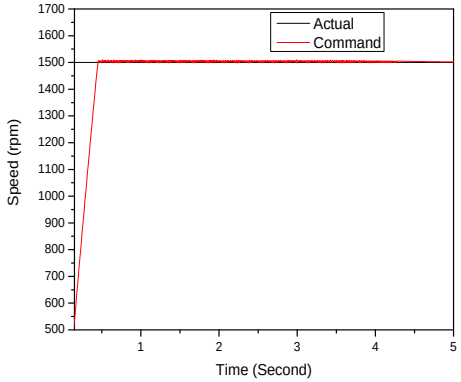

(b)

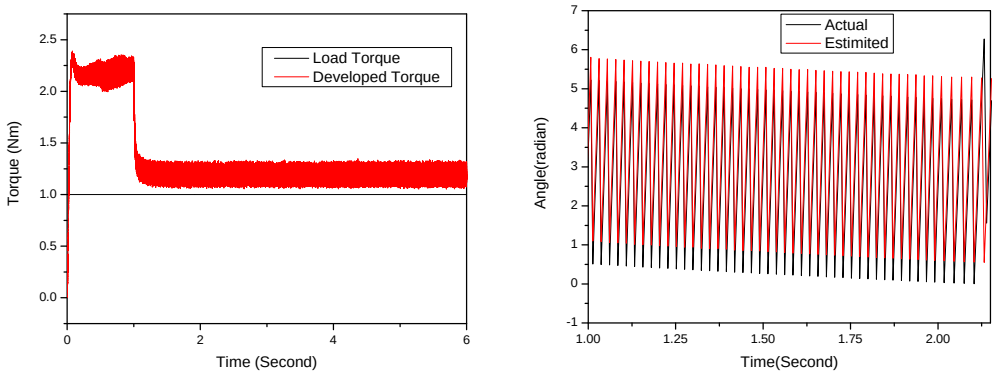

(c) (d)

Figure 5.11 (a) Estimated rotor angle, (b) Speed, (c) Developed electromagnetic torque, and (d) Three phase currents for the proposed IPMSM drive under speed ramp speed change by using GA

Ramp speed is also is an essential requirement for high performance IPMSM drives. The controller set speed response curve was gradually increased from zero and at time t=0.45 second it remained constant to 1500 rpm value. The estimated rotor position, speed response, developed electromagnetic torque and motor currents are shown in Fig. 5.11. The motor follows the command speed from the starting without any oscillation and steady- state error.

It is observed that GA based system needs t=0.45sec to speed up that motor at reference speed 1500 rpm, whereas Natural Algorithm based system needs t=1.0 sec.

5.4.5 Sudden Disturbance Torque

A sudden load disturbance (1.5 N.m) for a very short duration of 0.1 second was applied to the IPMSM drive. Fig. 5.12(a) shows the actual and estimated rotor angle of the motor at that time period. The speed response of the IPMSM is shown in Fig. 5.12(b). Simulation studies show that the proposed control scheme is still capable to estimate the rotor angle accurately. . The speed response curve reached to the command speed at t=0.45sec. Besides, the motor speed is insensitive to the sudden torque disturbance. Fig. 5.12(c) and (d) show the corresponding developed torque and motor currents.

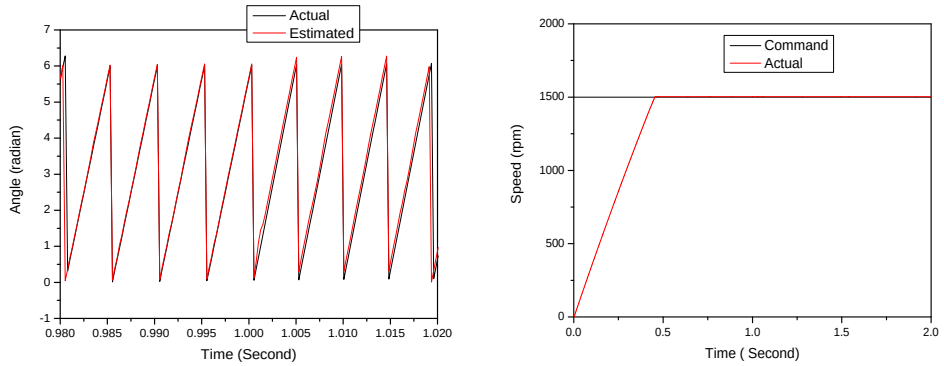

(a) (b)

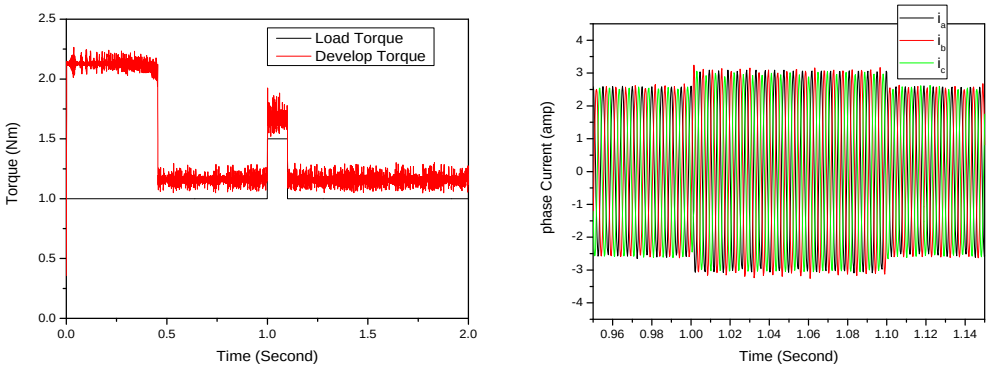

(c) (d)

Figure 5.12 (a) Estimated rotor angle, (b) Speed, (c) Developed electromagnetic torque, and (d) Three phase currents for the proposed IPMSM drive for sudden disturbance torque.

By applying GA,

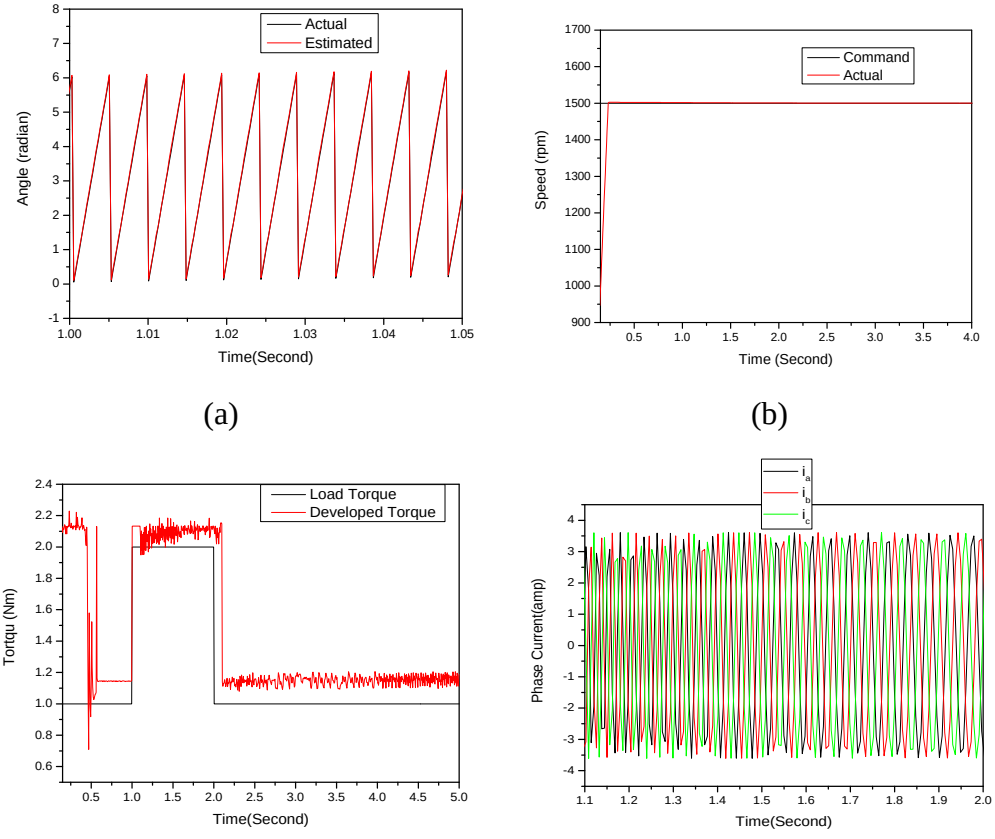

(a) (b)

(c) (d)

Figure 5.13 (a) Estimated rotor angle, (b) Speed, (c) Developed electromagnetic torque, and (d) Three phase currents for the proposed IPMSM drive for sudden disturbance torque by using GA.

A sudden load disturbance for a very short duration of 0.1 second was applied to the IPMSM drive. Fig. 5.13(a) shows the actual and estimated rotor angle of the motor at that time period. The speed response of the IPMSM is shown in Fig. 5.13(b). Simulation studies show that the proposed control scheme is still capable to estimate the rotor angle accurately. Besides, the motor speed is insensitive to the sudden torque disturbance. . The speed response curve reached to the command speed at t=0.23sec. Fig. 5.13(c) and (d) show the corresponding developed torque and motor currents.

It is observed that GA based system needs t=0.23sec to speed up that motor at reference speed 157 rpm, whereas Natural Algorithm based system needs t=0.45 sec.

5.4.6 Presence of Computational Errors

There is always instrumental error present in physical system. For the robustness test ±8% instrumental error was introduced to the inverter dc voltage. The estimated and actual rotor angle of the IPMSM is shown in Fig. 5.14(a). It is observed that the presence of computational error does not affect the estimation. The performance of motor speed, developed torque, and stator currents are presented in Fig. 5.14(b) to Fig. 5.14(d). The speed response curve reached to the command speed at t=0.45sec. Depending on the performance it can be claimed that the performance of the proposed control scheme is insensitive to the computational error within the range of -8% to 8%.

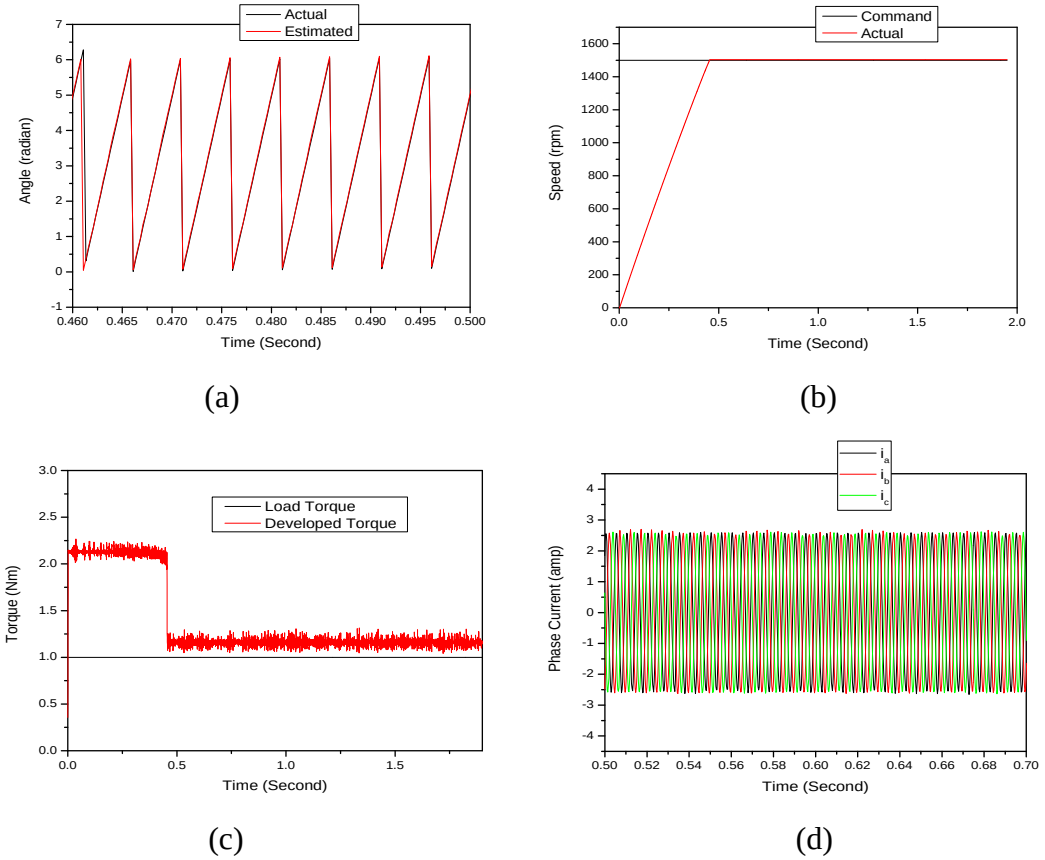

Figure 5.14 (a) Estimated rotor angle, (b) Speed, (c) Developed electromagnetic torque, and (d) Three phase currents for the proposed IPMSM drive for computational error.

By applying GA,

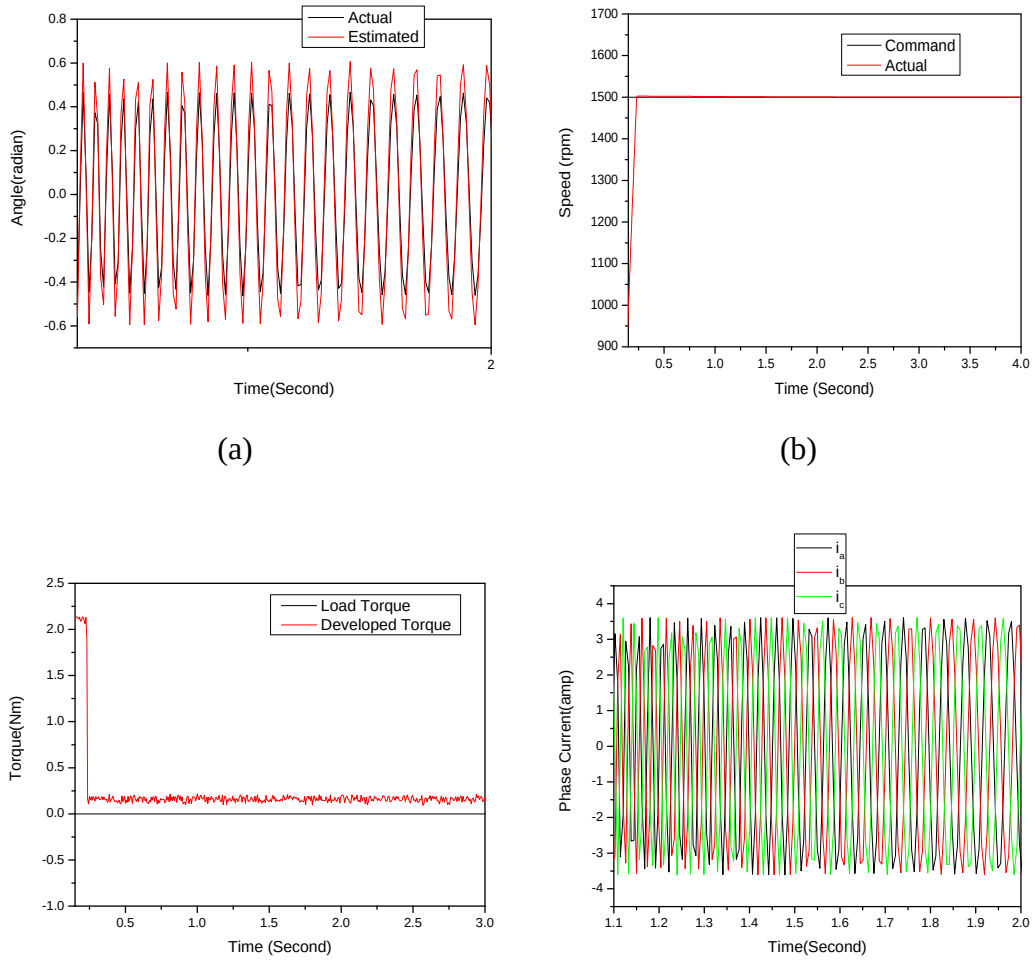

(a) (b)

(c) (d)

Figure 5.15 (a) Estimated rotor angle, (b) Speed, (c) Developed electromagnetic torque, and (d) Three phase currents for the proposed IPMSM drive for computational error by using GA.

The estimated and actual rotor angle of the IPMSM is shown in Fig. 5.15(a). It is observed that the presence of computational error does not affect the estimation. The performance of motor speed, developed torque, and stator currents are presented in Fig. 5.14(b) to Fig. 5.14(d). The speed response curve reached to the command speed at t=0.23sec.

It is observed that GA based system needs t=0.23sec to speed up that motor at reference speed 1500 rpm, whereas Natural Algorithm based system needs t=0.45 sec.

5.5 Conclusion

The performance of the IPMSM drive system in both transient and steady-state conditions will be improved with the use of 4S3P inverter and RTRNN based rotor position estimator. The drive system will be more reliable and cost effective. The speed response of the drive is expected to be faster by using GA than the previous IPMSM drives. The drive will also be robust to load disturbances, parameter variations, and speed reversal conditions. The absence of position sensor and reduced inverter size will make the drive system more attractive for industry applications.

A novel speed control technique based on a hybrid intelligent controller for an IPMSM drive has been presented in this Project. The PI controller parameters have been optimized by using a GA with a performance index to reflect the minimum settling time. The result observed very fast response of the IPMSM drive by applying the GA. The actual speed is very fast to reach the command speed. Very fast response of the system without oscillation indicates the effectiveness of the proposed control scheme.

The difference between the speed response curves of natural algorithm vs. genetic algorithm, GA is faster than natural algorithm. About a half time of natural algorithm, the GA's speed response curve reaches to the command speed.

CHAPTER VI

Conclusion and Proposed for Future Research

6.1 Conclusion

The objective of this Master's project was Evolutionary algorithm(EA) based high performance control of synchronous motor drive in which an effort was made to accommodate the robust and insensitive features of artificial neural network estimator. The total control law was designed on the consideration of field orientation control with magnetic saturation in synchronous motor drive. Step by step development, analysis and study of the proposed methodology have been done in different chapters. The simulation results demonstrate the acceptability of the proposed control methodology for high performance applications.

In this research work, PI controller based voltage vector controlled drive with Genetic Algorithm was used. It was demonstrated that the proposed GA based PI controller need less time to speed up the motor at transient condition and generate negligible speed fluctuation at rated speed under steady- state condition. The gain coefficients of PI controller in the proposed control system have been tuned by GA.

The work is presented in this dissertation used artificial neural network based flux estimation and suitable control law for high performance control of synchronous motor drive. For these purposes mathematical models of the three phase synchronous motor are written in d-q reference frame under different operating conditions. PI controller based field orientation model and control laws have been designed for the high performance controller. A saturation model of three phase synchronous motor was developed in the study to have more realistic study of the motor drive performance.

The artificial neural network based rotor flux estimator presented in this dissertation has been shown is very accurate and robust to parameter changes. It uses evolutionary algorithm learning based correlated α- and β- axes flux estimation and found to work satisfactorily under transient and steady- state conditions. Estimated flux components utilized to estimate the positions of the rotor flux axis also produce accurate results under steady state and transient conditions. The evolutionary algorithm learning has been accepted for flux and angle estimation in designing the high performance drive in this dissertation for its better performance.

The proposed control methodology originates from the speed and torque error processing through controllers instead of instantaneous switching. The proposed method generates the required voltage components which are used to find out the required voltage magnitude and its position from the inverter. The results of the proposed control system are compared with the control system having GA based PI controller. Very fast speed response, less torque pulsations and capo work under different operating conditions indicate the efficacy of the proposed control method. It has been observed that the proposed control method is robust against parameter changes and disturbances. The proposed GA based PI controller based ANN flux estimator can

be viewed as a part of an effective high performance controller. It is evident from the various simulation results carried out under varying operating conditions.

Based on the results from the previous chapters and the above discussion it can be concluded that the proposed control scheme provides high performance control for synchronous motor drives.

6.2 Proposed for Future Research

The dissertation presents a methodology to utilize the artificial intelligence in synchronous motor control. Different types of flux estimators may be proposed and studied by the researchers working in this area. Future researchers may try with fuzzy- neuro estimators with composite evolution algorithm learning based ANNs. Newly introduced training methods, such as particle swarm optimization or bacterial foraging technique may be tested for training the ANN- Fuzzy estimators. These flux estimators are expected to work effectively under all operating conditions with perturbed parameters. Controller based ob ANN- based synchronous motor model can be used to developed model reference control of synchronous motor. On line tuning of the motor model parameters using measurable variables is expected to produce designed results for which the control law is designed.

REFERENCES

[1] M. Nasir Uddin, Member, IEEE, M. A. Abido, Member, IEEE, and M. Azizur Rahman, Fellow, IEEE," Hybrid Intelligent Controller for Interior Permanent-Magnet Synchronous Motor Drives". IEEE Transactions on Industry Applications, vol. 40, no. 1, pp. 68-76, January/February 2004

[2] D. E. Goldberg, Genetic Algorithms in Search, Optimization, and Machine Learning. Reading, MA: Addison-Wesley, 1989.

[3] A. Accetta, M. Cirrincione, and M. Pucci, "Sensorless Control of PMSM by a Linear Neural Network: TLS EXIN Neuron", Proceedings of the Annual Conference on IEEE Industrial Electronics Society, pp. 974-978, Glendale, USA, 2010.

[4] T. Sebastian, G. Slemon, and M. Rahman, "Modelling of permanent magnet synchronous motors," Magnetics, IEEE Transactions on, vol. 22, pp. 1069-1071, 1986.

[5] T. M. Jahns, G. B.Kliman, and T. W. Neumann, "Interior Permanent-Magnet Synchronous Motors for Adjustable-Speed Drives," Industrial Applications, IEEE Transactions on, vol. IA-22, pp. 738-746, 1986.

[6] P. Pillay and R. Krishnan, "Modeling of permanent magnet motor drives," Industrial Electronics, IEEE Transactions on, vol. 35, pp. 537-541, 1988.

[7] P. Pillay and R. Krishnan, "Modeling, simulation, and analysis of permanent-magnet motor drives. I. The permanent-magnet synchronous motor drive," Industry Applications, IEEE Transactions on, vol. 25, pp. 265-273, 1989.

[8] S. Morimoto, Y. Tong, Y. Takeda, and T. Hirasa, "Loss minimization control of permanent magnet synchronous motor drives," Industrial Electronics, IEEE Transactions on, vol. 41, pp. 511-517, 1994.

[9] A. H. Wijenayake and P. B. Schmidt, "Modeling and analysis of permanent magnet synchronous motor by taking saturation and core loss into account," 1997.

[10] K. Jang-Mok and S. Seung-Ki, "Speed control of interior permanent magnet synchronous motor drive for the flux weakening operation," Industry Applications, IEEE Transactions on, vol. 33, pp. 43-48, 1997.

[11] B. K. Bose, Modern power electronics and AC drives: Prentice Hall, 2002.

[12] B. Cui, J. Zhou, and Z. Ren, "Modeling and simulation of permanent magnet synchronous motor drives," 2001.

[13] C. Mademlis and N. Margaris, "Loss minimization in vector-controlled interior permanent-magnet synchronous motor drives," Industrial Electronics, IEEE Transactions on, vol. 49, pp. 1344-1347, 2002.

[14] X. Jian-Xin, S. K. Panda, P. Ya-Jun, L. Tong Heng, and B. H. Lam, "A modular control scheme for PMSM speed control with pulsating torque minimization," Industrial Electronics, IEEE Transactions on, vol. 51, pp. 526-536, 2004.

[15] S. Onoda and A. Emadi, "PSIM-based modeling of automotive power systems: conventional, electric, and hybrid electric vehicles," Vehicular Technology, IEEE Transactions on, vol. 53, pp. 390-400, 2004.

[16] G. Venkaterama, "Simulink Permanent Magnet Simulation," University of Wisconsin.

[17] Mathlab-Works-Support, "PM Synchronous Motor Drive," http://www.mathworks.com/access/helpdesk/help/toolbox/physmod/powersys/powersys.html.

[18] R. Krishnan, Electric Motor Drives Modeling, Analysis, and Control Pearson Education, 2001.

[19] B. K. Bose, Modern power electronics and AC drives: Prentice Hall, 2002.

[20] B. K. Bose, Power Electronics and Variable Frequency Drives, 1 ed: Wiley, John & Sons, 1996.

[21] M. Aydin, "Axial Flux Mounted Permanent Magnet Disk Motors For Smooth Torque Traction Drive Application," in Electrical and Computer Engineering, vol. PhD: University of Wisconsin 2004, pp. 453.

[22] A. Khurram, 2001,"Position and speed sensorless control of permanent magnet synchronous motors," phD dissertation, Michigan State University, East Lansing, USA.

[23] Valkenburg, Nooger, and Neville, 1992, "Basic Electricity", Indianapolis, IN: Prompt Publication, Revised Edition.

[24] P. C. Krause, Analysis of EIectric Machinery, McGraw-Hill Inc., 1986.

[25] T. Sebastian, G. R. Slemon and M. A. Rahman, 'Modelling of Permanent Magnet Synchronous Motors", EEE Truns. on Magnetics, vol. MAG-22, no. 5, 1986, pp. 129-134.

[26] F. J. Lin, R. I. Wai and H. P. Chen, "A PM Synchronous Servo Motor Drive with an On-Line Trained Fuay Neural Network Controller", IEEE Tram. on Energy Conversion, vol. 13, no. 4, December 1998, pp. 319-325.

[27] B. K. Bose, Modern power electronics and AC drives: Prentice Hall, 2002.

[28] Shady. M. Gadoue, D. Giaous and J. W. Finch, 'Genetic Algorithm Optimized PI and Fuzzy Mode Speed Control for DTC drives', Proceedings of the World Congress on Engineering 2007, Vol. 1, WCE 2007, July 2-4, 2007, London, U.K.

[29] R. Anulmozhiyal and Dr. K. Baskarn, 'Speed Control of Induction Motor Using Fuzzy PI and Optimized Using GA', International Journal of Recent Trends in Engineering, Vol. 2, No. 5, November 2009

[30] Neenu Thomas, Dr. P. Poongodi, 'Position Control of DC Motor Using Genetic Algorithm-based PID Controller', Proceedings of the World Congress on Engineering 2009, Vol. 2, WCE 2009, July 1-3, 2009, London, U.K.

[31] Jin-Sung Kim, Jin-Hwan Kim, Ji-Mo Park, Sung-Man Park, Won-Yong Choe and Hoon Heo 'Auto Tuning PID Controller Based on Improved Genetic Algorithm for Reverse Osmosis Plant', World Academy of Science, Engineering and Technology 47 2008

[32] Watanabe**,** Keigo, Hashem, M.M.A. 2004, XIX, "New Algorithms and their Applications to Evolutionary Robots Series",Studies in Fuzziness and Soft Computing, Vol.147, 172 p.

[33] M.N.Uddin, T.S.Radwan, and M.A.Rahman,2006, " Fuzzy-logic- controller- based cost effective four- switch three- phase inverter- fed IPM synchronous motor drive system," IEEE Trans. On Industry Applications, Vol.42,No.1, pp.21-30

[34] T. O. Mahony, C. J. Dowing and K. Fatla, 'Genetic Algorithm for PID Parameter Optimization: Minimizing Error Criteria', Process Control and Instrumentation, 2000, 26-28 July 2000, University of Stracthclyde, pp. 148-153

[35] Simon Haykin,2001,"Neural Networks aComprehensive Foundation," 2nd edition, pearson education, Inc.

[36] Md. Abdur Rafiq, Mohammed Golam Sarwer, & B.C. Ghosh, "Fast Speed Response Field-Orientation Control of Induction Motor Drive with Adaptive Neural Integrator," Istanbul University-Journal of Electrical & Electronics Engineering, Vol. 6, No: 2, pp. 229-235, 2006.

[37] S. Bologani, G. S. Buja, 1985," Control System Design of a Currernt Inverter Induction Motor Drives" IEEE Trans. On Industry Applications, Vol. IA-21.5, pp. 1145-1153.

[38] A. Tripathi and P. C. Sen, Comparative analysis of fixed and sinusoidal band hysteresis current controller for voltage source inverters", IEEE Trans. on Ind. Elect, vol. 39, Feb. 1992, pp. 63-73.

APPENDIX

APPENDIX- A

IPMSM Parameters

Number of phases = 3
Number of poles = 4
Rated frequency = 60 Hz
Rated power = 1 hp
Rated input line to h e voltage= 208 V
q-axis inductance L_q = 0.07957 H
d-axis inductance L_d = 0.04244 H
Stator resistance per phase r_s = 1.93 Ω
Inertia constant J_m = 0.003 Kg.m^2
Rotor damping constant B_m= 0.0008 (N-m)/rad./sec.
Permanent magnet flux linkage ψ_m = 0.3 14 volt/rad./sec.
Magnet type = Samarium Cobalt.

Speed loop: Kp = 0.04, Ki = 10.0

Weight of the RNN: $W_1 = W_2 = 0.1$, $W_1 = W_2 = 0.0001$, : $W_1 = W_2 = 0.068$,
$W_1 = W_2 = -0.05$, $W_1 = W_2 = 0.0001$,